AFRL-PR-WP-TR-2006-2211

ADVANCED FUEL DEVELOPMENT AND FUEL COMBUSTION

Delivery Order 0007: Abatement of Soot from Military Gas Turbine Engines via Fuel Additives

Prof. Thomas A. Litzinger

Pennsylvania State University
248 Calder Way
University Park, PA 16802

AUGUST 2006

Final Report for 01 February 2001 – 31 August 2006

Approved for public release; distribution is unlimited.

STINFO COPY

PROPULSION DIRECTORATE
AIR FORCE MATERIEL COMMAND
AIR FORCE RESEARCH LABORATORY
WRIGHT-PATTERSON AIR FORCE BASE, OH 45433-7251

NOTICE AND SIGNATURE PAGE

This report was cleared for public release by the Air Force Research Laboratory Wright Site (AFRL/WS) Public Affairs Office and is available to the general public, including foreign nationals. Copies may be obtained from the Defense Technical Information Center (DTIC) (http://www.dtic.mil).

AFRL-PR-WP-TR-2006-2211 HAS BEEN REVIEWED AND IS APPROVED FOR PUBLICATION IN ACCORDANCE WITH ASSIGNED DISTRIBUTION STATEMENT.

*//Signature//
ROBERT PAWLIK, 1st USAF
Project Monitor
Combustion Branch

//Signature//
ROBERT D. HANCOCK, Ph.D.
Chief
Combustion Branch

//Signature//
JEFFREY M. STRICKER
Chief Engineer
Turbine Engine Division
Propulsion Directorate

*Disseminated copies will show "//Signature//" stamped or typed above the signature blocks.

REPORT DOCUMENTATION PAGE	*Form Approved* *OMB No. 0704-0188*

1. REPORT DATE ***(DD-MM-YY)*** August 2006	**2. REPORT TYPE** Final	**3. DATES COVERED *(From - To)*** 02/01/2001 – 08/31/2006

4. TITLE AND SUBTITLE ADVANCED FUEL DEVELOPMENT AND FUEL COMBUSTION Delivery Order 0007: Abatement of Soot from Military Gas Turbine Engines via Fuel Additives	**5a. CONTRACT NUMBER** F33615-98-D-2802-0007
	5b. GRANT NUMBER
	5c. PROGRAM ELEMENT NUMBER 62203F
6. AUTHOR(S) Prof. Thomas A. Litzinger	**5d. PROJECT NUMBER** 3048
	5e. TASK NUMBER 05
	5f. WORK UNIT NUMBER EX
7. PERFORMING ORGANIZATION NAME(S) AND ADDRESS(ES) Pennsylvania State University 248 Calder Way University Park, PA 16802	**8. PERFORMING ORGANIZATION REPORT NUMBER**
9. SPONSORING/MONITORING AGENCY NAME(S) AND ADDRESS(ES) Propulsion Directorate Air Force Research Laboratory Air Force Materiel Command Wright-Patterson AFB, OH 45433-7251	**10. SPONSORING/MONITORING AGENCY ACRONYM(S)** AFRL-PR-WP
	11. SPONSORING/MONITORING AGENCY REPORT NUMBER(S) AFRL-PR-WP-TR-2006-2211

12. DISTRIBUTION/AVAILABILITY STATEMENT

Approved for public release; distribution is unlimited.

13. SUPPLEMENTARY NOTES

PAO case number: AFRL/WS 06-2294; Date cleared: 27 Sep 2006. This report contains color.

14. ABSTRACT

The technical objective of this program was to develop fundamental understanding of the complex interactions of additives with the processes that lead to PM emissions from military gas turbine engines and to use that fundamental understanding to select and investigate the most promising additives for reducing PM emissions. Because of the inherent complexity of the combustion processes within gas turbine combustors and great difficulty in making measurements inside combustors, it was not possible to achieve the technical objective of this program by making measurements in gas turbine combustors. Furthermore, due to the complexity of the combustion process in a gas turbine combustor, no single laboratory flame or reactor will suffice as a model for a combustor. Therefore, multiple laboratory devices were applied to study the effects of additives on soot formation processes. These devices included a shock tube, a well-stirred reactor, premixed flames, diffusion flames, a spray flame, and a high pressure turbulent reactor. Experiments were performed at Penn State in four of these devices: a premixed flame, a co-flow diffusion flame, a spray flame and the high pressure turbulent reactor.

15. SUBJECT TERMS

soot, emissions, PAH, polycyclic aromatic hydrocarbons, combustion, combustors, fuel additives, soot formation processes, premixed flame, co-flow flame, spray flame, high pressure turbulent reactor

16. SECURITY CLASSIFICATION OF:			**17. LIMITATION OF ABSTRACT:**	**18. NUMBER OF PAGES**	**19a. NAME OF RESPONSIBLE PERSON** (Monitor)
a. REPORT	**b. ABSTRACT**	**c. THIS PAGE**			1st Lt Robert Pawlik
Unclassified	Unclassified	Unclassified	SAR	92	**19b. TELEPHONE NUMBER** *(Include Area Code)* N/A

Standard Form 298 (Rev. 8-98)
Prescribed by ANSI Std. Z39-18

1. EXECUTIVE SUMMARY

The technical objective of this program was to develop fundamental understanding of the complex interactions of additives with the processes that lead to particulate matter (PM) emissions from gas turbine engines and to use that fundamental understanding to select and investigate the most promising additives for reducing PM emissions. Because of the inherent complexity of the combustion processes within gas turbine combustors and great difficulty in making measurements inside combustors, it was not possible to achieve the technical objective of this program by making measurements in gas turbine combustors. Furthermore, due to the complexity of the combustion process in a gas turbine combustor, no single laboratory flame or reactor will suffice as a model for a combustor. Therefore, multiple laboratory devices were applied to study the effects of additives on soot formation processes. These devices included a shock tube, a well-stirred reactor, premixed flames, diffusion flames, a spray flame, and a high pressure turbulent reactor. Experiments were performed at Penn State in four of these devices: a premixed flame, a co-flow diffusion flame, a spray flame and the high pressure turbulent reactor.

Numerical simulation proved to be an invaluable tool for understanding the mechanisms by which additives reduce soot in the laboratory flames and reactors. Extensive simulations were performed for the premixed flame to understand the effects of oxygenated compounds and NO_2 on soot. The major limitation was typically the availability of an appropriate kinetic mechanism for the additive; however, transport and thermodynamics properties were sometimes an issue as well. A new mechanism for ethanol, di-methyl ether, and ethylene was created as part of this work.

Over the course of this program, three different classes of organic compounds, oxygenates, nitro-alkanes, and nitrogen-heterocycles, were investigated along with phosphorus. Three primary mechanisms through which these compounds affected soot were uncovered through the course of the program:

1. changing the temperature in the fuel-rich, soot formation regions
2. decreasing the production rates of aromatic species
3. increasing the number of C-atoms involved up in strong chemical bonds such as C-O or C-N

The temperature/thermal effect can be very significant but is also variable so this effect can be complex. As reaction temperature increases, soot production will increase initially, reach a maximum and then decrease. At low temperatures, soot formation, increases due to increasing rates of production of soot precursor species, but at elevated temperatures, soot formation decreases due to the thermal instability of the aromatic structure and key radical intermediary adducts. Hence at low temperatures, increasing temperatures increase soot production, but at high temperatures, the converse is true. An additive can shift reaction temperatures by delaying or accelerating heat release rates, or by changing the peak flame (equilibrium) temperatures. Because of these complex dependencies, this temperature effect proved to be one of the most important to understand first when comparing relative effects across the suite of devices that were used in the study.

Perhaps the most important characteristic of an additive in reducing the production rate of aromatics (and hence soot) is its ability to decrease the concentration of the propargyl radical (C_3H_3). Propargyl is known to be a key intermediate in the production of benzene (C_6H_6), the smallest aromatic species. Alternatively, increases in this radical will increase benzene and hence soot production. The very significant role of this single species can be recognized via the squared dependency of the rate of aromatic production on its concentration, i.e.,

$$C_3H_3 + C_3H_3 \rightarrow C_6H_5 + H \text{ (or } C_6H_6\text{)}$$
$$d\{C_6H_5\}/dt = k\,[C_3H_3]^2$$

Through the course of the study evidence was also found that changes in “even-carbon” pathways to formation of the first aromatic ring, e.g., $C_4H_5 + C_2H_2$, can also be important under certain conditions.

Finally the presence of strong chemical bonds between carbon and oxygen or nitrogen were found to be important. Once bound in such strong bonds, these carbon atoms are not available to the carbon pool that can lead to soot production. Also, the program produced some evidence that nitrogen embedded in an aromatic ring can tie up all the carbon in that ring (e.g. pyridine) at least for a period of time leading to a reduction in the formation of aromatic species that are the building blocks of soot.

The following sections summarize findings for each additive. It is important to note that the relative roles of the above soot-reducing mechanisms can change for any single additive, depending on the experimental apparatus, fuel type or experimental conditions. In fact such changes can be so dramatic that in one case, soot is decreased through the use of a selected additive but causes an increase or no change under other conditions. Such observed contrary effects have been commonly reported in the literature. This program has contributed significantly to the fundamental understanding of the chemistry behind such seemingly contradictory trends.

Oxygenated Compounds

The initial work on oxygenated additives focused on ethanol and its effect during the combustion of ethylene. To investigate effects of additive structure in soot reduction, experiments were also conducted in the premixed flame with dimethyl ether (DME). After completion of the ethylene studies, studies with liquid fuels were undertaken. In addition to ethanol and DME, cyclohexanone was studied because it was a component in a commercial additive that produced some soot reduction.

Through detailed modeling studies, the mechanism by which soot is increased when ethanol is added to ethylene in the opposed jet diffusion flame was determined to be kinetic in nature as well. Soot was increased due to the enhancement of the “even-carbon species” pathway to benzene as a result of the production of methyl radicals from ethanol, not via the enhancement of the “odd-carbon species,” as was originally expected. Detailed modeling of the results for DME and ethanol addition to the ethylene diffusion flames demonstrated that the reduction in these flames is via effects on the propargyl radical route to the first aromatic ring. These studies also demonstrated that the chemical structure of the additive does play a role in the effectiveness of oxygenated additives in reducing soot.

Due to its cyclic structure, cyclohexanone appeared to have the potential to remove six carbons from pathways to soot formation. It was studied in the various experimental test rigs to determine if it showed unusual effectiveness, which would lend credence to the hypothesis. However, its effectiveness was essentially the same as that of ethanol indicating that the mechanisms by which it reduced soot was likely the same as that of ethanol. A chemical kinetic mechanism was not readily available for this compound so detailed modeling was not pursued.

Nitro-alkane Compounds

The commercial additive that was found to be effective in reducing soot was determined to be composed to nitro-alkanes, cyclohexanone, toluene, and dichloroethane. The latter two compounds are known to increase soot so they were not investigated as possible additives. Cyclohexanone, as discussed above, is not unusually effective in reducing soot, so the nitro-alkanes, the primary constituents in the commercial additive, were identified as the likely constituents leading to soot reduction. Consequently, these compounds were investigated in detail with experiments and modeling; the three compounds investigated were nitromethane, nitroethane, and nitropropane.

In the various test rigs, the nitro-alkanes showed very complex effects on soot depending on experimental conditions and the structure of the additive. In the atmospheric pressure spray flame and the high pressure turbulent combustor the additives reduced soot, and their effect was dependent on the structure of the alkyl group. Unfortunately, the ability to simulate these complex flames was limited so no modeling could be done.

The NO_2 formed in the decomposition of the nitro-alkanes was identified as a key intermediate species in soot reduction so a study was undertaken in the premixed flame in an attempt to identify its role. The premixed flame study yielded the very interesting and unexpected result that soot decreased even though polycyclic aromatic species increased. Detailed modeling was used to understand this trend.

Nitrogen-heterocycles

The effectiveness of the nitro-alkanes led to consideration of other nitrogen containing species as potential additives. Results available in the literature indicated that pyridine produces much less soot than benzene suggesting that the presence of the ring-nitrogen is inhibiting soot formation. A possible mechanism for this effect is that the presence of the nitrogen in the ring is interrupting the addition of acetylene to the ring that is viewed as the major pathway to produce large aromatic species and soot. Pyridine was selected as the primary nitrogen-heterocycle for investigation.

Results from the addition of pyridine to the the turbulent spray flame showed substantial reductions in soot. However, experiments in the high pressure turbulent reactor showed no effect on soot when the fuel was JP8. At the suggestion of the SERDP Review Board, experiments were also run with heptane/toluene to check whether fuel effects might be the reason for the fact that pyridine had no effect on soot in the high pressure turbulent reactor. The experiments again showed no effect, so the divergent results remain unexplained. Again, modeling could not assist in understanding these trends due to an inability to model the spray flame and the turbulent reactor.

Phosphorus

The studies of the effects of phosphorus were done under supplemental funding for the program; therefore, the work performed was essentially screening studies to determine if the phosphorus showed sufficient reductions in soot to merit more detailed testing. Experiments were performed the premixed flame and in a co-flow diffusion flame because this type of flame was used in the prior study at NBS that motivated the investigation. Overall the results from the experiments are not encouraging in terms of the potential of phosphorus to reduce soot.

2. **RESEARCH METHODOLOGIES**

Due to the complexity of the combustion process in a gas turbine combustor, no single laboratory flame or reactor will suffice as a model for a combustor. Therefore, multiple laboratory devices were applied to study the effects of additives on soot formation processes. These devices included a shock tube, a well-stirred reactor, premixed flames, diffusion flames, a spray flame, and a high pressure turbulent reactor. Figure 2.1 shows the hierarchy of the devices in order of increasing complexity. Experiments were performed at Penn State in four of these devices: a premixed flame, a co-flow diffusion flame, a spray flame and the high pressure turbulent reactor.

This chapter presents summaries of the research methodologies applied. It includes descriptions of the various devices used in the study along with the associated measurement methods. The basic computational methods are also summarized.

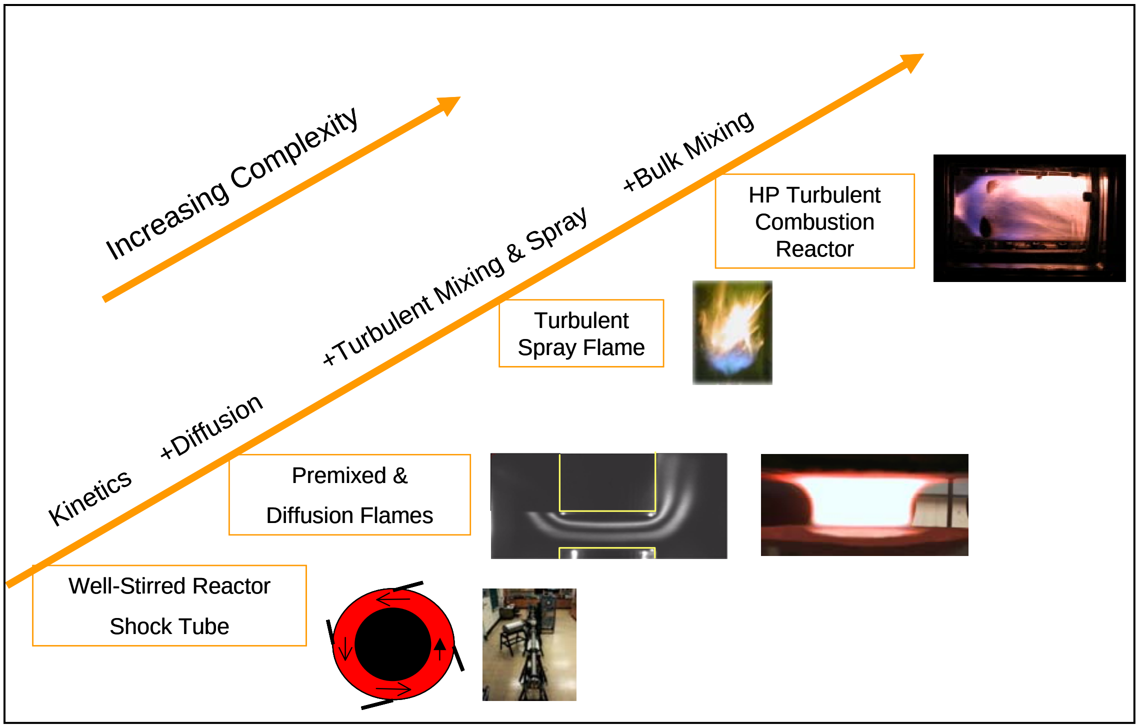

Figure 2.1: Hierarchy of devices used in this study

2.1 EXPERIMENTAL

2.1.1 PREMIXED FLAME

An unconfined flat laminar premixed flame was established using a commercial McKenna Burner with a 60.2-mm-diameter water-cooled porous-plate. The flame was stabilized using a flat plate. To facilitate measurements of profiles using line-of-sight optical methods, the burner could be moved in vertical direction with a precision of 100 μm, using an adjustable jack. The air, fuel and additive delivery systems are illustrated in Figure 2.2. The air to the burner was metered with rotameter, and the flow rate of fuel was controlled by a mass flow meter. The rotameter and mass flow meter were calibrated with bubble meters. Additives, which were supplied by a precision syringe pump, were vaporized and mixed with the fuel in a vaporizer. The temperature of the vaporizer was maintained at 80ºC by electric heating tape, which is controlled by an Omega temperature controller.

Two mixing processes occurred in turn: first, fuel mixed with additive in the vaporizer; after that, the fuel/additive mixture mixed with preheated air in a 160-cm-long mixing chamber. The mixing chamber consists of five equally spaced orifices mounted inside the chamber, and the mixing chamber length-to-diameter ratio was roughly 80 in order to attain fully mixed conditions. To prevent condensation of the ethanol, the mixing chamber and fuel tube were heated with five heating tapes. By varying the electric voltage applied to the heating tapes, the temperature of the flow at the inlet of the burner was maintained at 53ºC for all mixtures regardless of whether a liquid additive was introduced. This approach ensures that all the flames were established at the same ambient condition.

Measurement Methods

A variety of diagnostic methods were applied to these flames including laser-induced incandescence (LII) and extinction for soot, laser induced fluorescence for polycyclic aromatic hydrocarbons (PAH), and thermocouples for temperature measurements. Figures 2.3 illustrates the configurations of the equipment used in these measurements. In studies using NO_2, thermocouples were of limited use due to the chance of catalytic reactions of the NO_2 on the thermocouple; therefore, alternative methods including potassium line reversal were applied.

Laser-induced Incandescence (LII) was applied to obtain the spatial distribution of soot volume fractions in the flames; the set-up for this system is illustrated in Figure 2.3. A doubled Nd:YAG laser (Surelite, Continuum) of 532 nm operating at 10 Hz was used to irradiate the soot particles. The induced incandescence at 90 degree to the incident beam was imaged with a 105 mm UV camera lens (Nikon,f/4.5) onto an intensified charge coupled device (ICCD) camera (Princeton Instruments, Model ICCD 576S/RB). The camera gate time was set as 80 ns to include the laser pulse duration. A narrow band interference filter with a wavelength range of 425-435 nm was placed in front of the camera to prevent laser light scattering from soot particles from reaching the detector and to reject most background luminosity and laser induced fluorescence. LII signals can be categorized into two distinct regimes depending on the laser energy fluence, i.e., a linear regime with respect to the laser energy fluence and a saturated regime in which the signal is independent of the laser energy fluence (Ni et al., 1995). In present study, the laser pulse energy fluence was measured approximately to be 0.6 J/cm^2, which is in the saturated LII regime. LII images were acquired by averaging over 300 laser pulses. The statistical uncertainties in the soot volume fractions derived from the LII measurements were less than 5%.

Laser extinction measurement was used to calibrate the LII signals to obtain absolute local soot volume fraction. The extinction measurements were made using an Argon ion laser and a chopper (1KHz) lock-in amplifier. Since the flame was quite uniform in the radial direction and edge effects were negligible, data collection was simplified by taking line-of-sight average absorption measurements through the center of the flame. The 514.5 nm laser beam was focused onto the flame using a 1-m focal length lens and was received by a Silicon photodiode detector. Because the location of the laser beam on the detector surface fluctuated due to the large temperature gradient across the flame, an additional shorter focal length lens was employed to focus the laser beam to maintain its location on an area of a photodiode detector, over which variations in sensitivity were small. The system was calibrated against a series of Standard Natural Density Filters and the linearity was better than 99%. Data were recorded using a National Instruments data acquisition system (NI-PCI-6110) with a sampling rate of 1000 samples/sec; the mean voltage value was obtained by averaging over a period of one minute.

Aromatic species were measured using laser-induced fluorescence following the work of Sgro *et al*. (2001). The LIF signal of PAH was produced by employing the fourth harmonic wavelength of Nd:YAG at 266 nm. The UV beam of 266 nm excites both small aromatic species and large PAH species. During the development of the method, the broadband spectral characteristics of the fluorescence were observed using a 1/4-meter spectrometer (GCA-McPherson EU-700) over the spectral region from 250 to 600 nm, corrected by spectrometer efficiency. On an optical axis perpendicular to the laser beam, a 100 mm focal length UV lens collected light over an 8 mm length of the beam in the flame and focused the image onto the entrance slit of the spectrometer. Calibration using a 6035 Hg(Ar) lamp showed that the spectrometer had a resolution of 5 nm with a 0.4-mm-wide slit, which was positioned parallel to the propagation direction of the laser beam. The spectrometer was automatically driven by a Labview program at 5 nm/min. The signal from the photomultiplier (RCA Model 4840), which operated at 800 V, was processed by a BOXCAR and recorded using the NI data acquisition system with a sampling rate of 1000 samples/sec.

Wavelength bands for the collection of fluorescence characteristic of small aromatic species and large PAH were selected based on the work of Beretta *et al.* (1992). who assigned the UV fluorescence to small aromatic species of one or two rings and the visible fluorescence to larger PAH. For small aromatic species a combination of a 320 nm cutoff filter (WG320) and a UV pass filter (UG11) were used to collect the fluorescence in the wavelength range between 320 and 380 nm. For large PAH of three or more rings the wavelength range from 420 to 480 nm was observed using a combination of high pass filter (GG420) and low pass filter (BG12). The camera was gated on for 35 ns during the laser pulse. Fluorescence from 500 laser pulses was accumulated to generate a PAH LIF intensity profile. Obtaining quantitative information from the LIF technique is difficult due to quenching, broadening of the absorption line, absorption of incident light and the self-absorption of fluorescence. No feasible method of calibration was found, so only relative concentration results of PAH are presented.

Temperature profiles for each flame were measured using traditional thermocouple method. The probe configuration and methodology used were those of McEnally *et al.* (1997) The thermocouple was uncoated, pre-welded type R (Pt/Pt-13%Rh) wire pairs. The junction was nearly spherical. Diameters of wire and junction bead are approximately 76µm (0.003 inch) and 239µm, respectively. The starting point for the temperature measurement was 2mm above the burner surface, and temperatures were measured at 0.5mm spacing intervals near the main reaction zone, where the temperature gradient is steep. In the post-flame zone where the temperatures were changing more slowly, temperature was measured with 1mm or 2mm intervals up to a maximum height of 20 mm. The average insertion time to reach the final position was approximately 400ms. Data points were recorded on IBM compatible PC using commercial LABVIEW software. The final junction temperature was obtained from a linear extrapolation of the temperature history to time zero, representing the moment when the junction reached its final position. Temperatures presented in this paper were corrected for heat loss, following the methodology of Shaddix. (1999).

For the studies using NO_2, potassium line reversal was used to measure temperature in the non-sooting regions, enabling measurements far closer to the burner surface than possible with more traditional techniques such as thermocouples. The line reversal technique or the sodium D-line reversal technique, as it is more widely known, is based on the following principle. The flame is seeded with sodium atoms using a suitable seeding method. The seeded sodium atoms have to be in local thermodynamic equilibrium with the hot gases in the flame. As a result of the increased temperature due to the combustion process, the outer electron in the sodium atom will be excited from the ground state to a higher resonance level. The excited sodium atoms will emit radiation at the characteristic emission wavelengths, particularly in the D-line or the doublet consisting of the 589 and 589.9 nm emission lines. The intensity of the emitted signal is proportional to the population of the excited sodium atoms as well as the local temperature of the hot gases.

The true temperature of the hot gases can be measured by comparing the emission signal intensity against a calibrated background continuum source using a combination of a spectrometer and an optical detector array. The typical light source is usually in the form of a tungsten lamp, calibrated for apparent temperature of the tungsten filament against lamp current. When the temperature of the lamp filament is lower than that of the flame, the D-line will still be in emission. But the D-line will go into absorption when the lamp temperature is higher than that of the local flame temperature. The apparent temperature of the lamp filament will be equal to the true local temperature of the flame when the intensity of the emission line is equal to the intensity of the background continuum at the same wavelength. The same principle holds true for other alkali metals such as lithium and potassium.

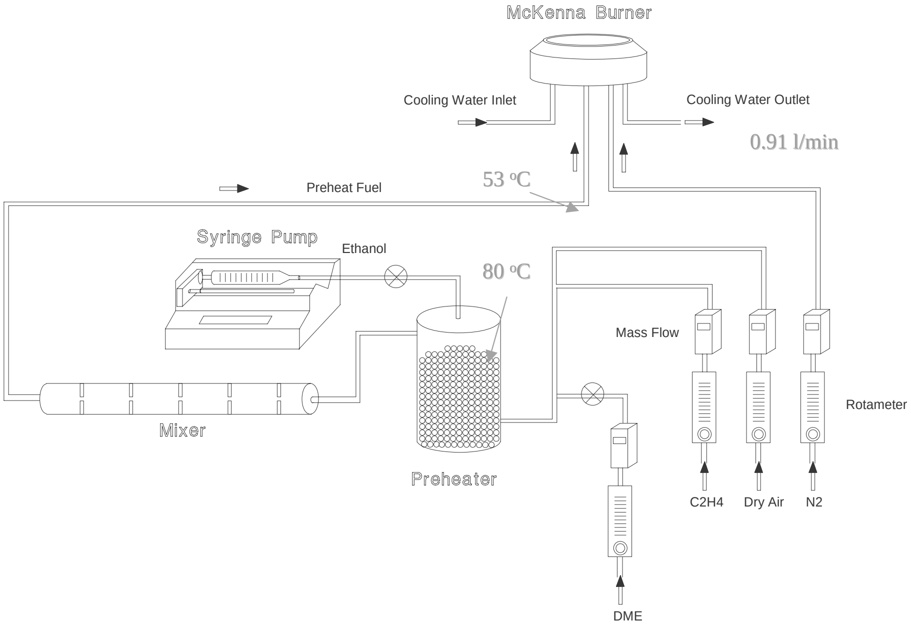

Figure 2.2. Schematic of fuel, additive, and air delivery systems for premixed flame experiments at Penn State

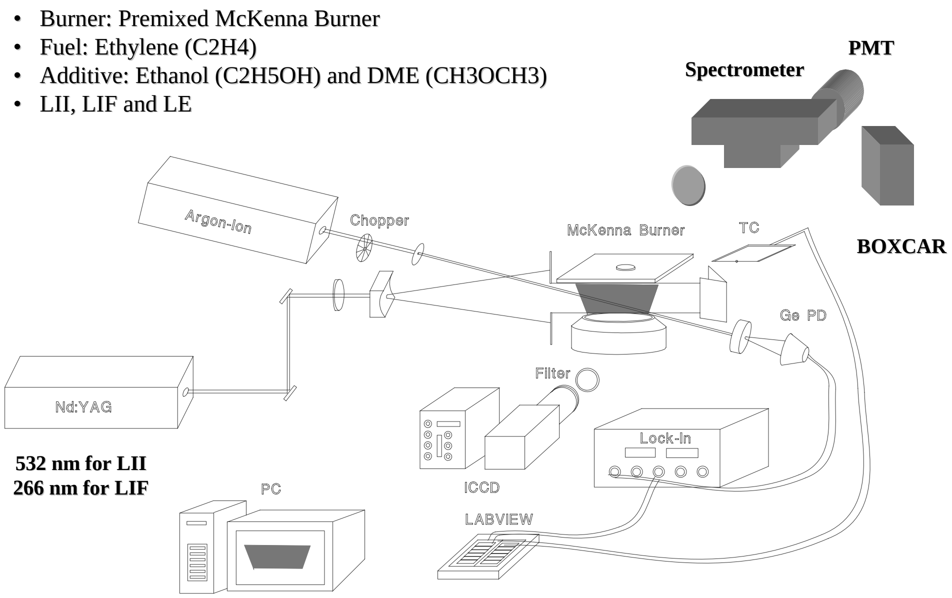

- Burner: Premixed McKenna Burner
- Fuel: Ethylene (C2H4)
- Additive: Ethanol (C2H5OH) and DME (CH3OCH3)
- LII, LIF and LE

Figure 2.3: Experimental set-up for measurements of soot and PAH

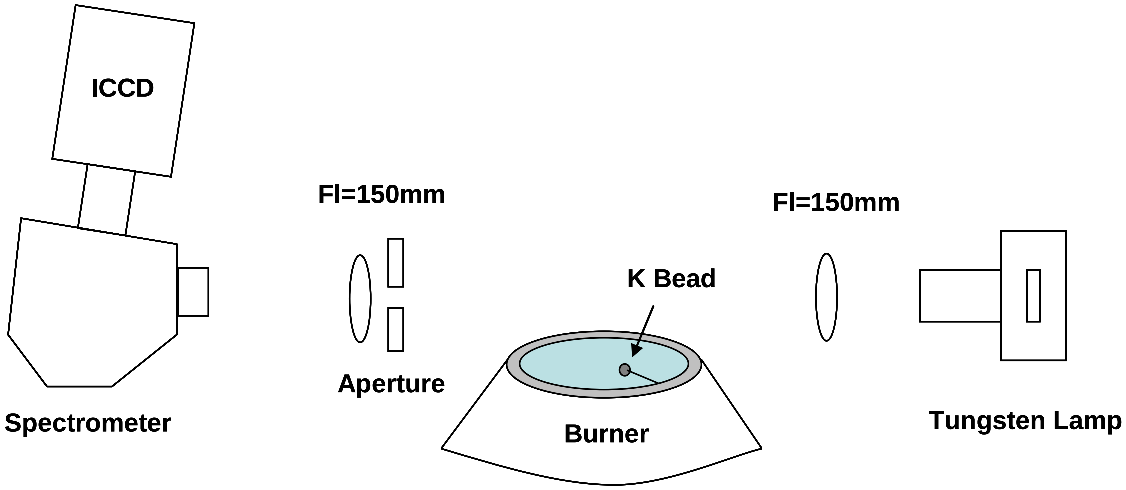

Figure 2.4. Schematic of line reversal technique. The potassium (K) at 770 nm is seeded in the flame.

2.1.2 *CO-FLOW DIFFUSION FLAME*

The co-flow diffusion flame was not part of the suite of burners used in the original study. It was included in the program only for the study of phosphorus which was an 'add-on' to the original program. The co-flow diffusion flame was included because the work of Hastie and Bonnell (1980), which motivated the phosphorus work, included experiments in a small scale, co-flow diffusion flame.

The co-annular laminar diffusion flame burner that was used is described in detail by Santoro *et al*. (1983), who designed and fabricated the original burner on which the one used in this study is modeled. The burner consists of an inner brass fuel tube of 10.8 mm inner diameter surrounded by an outer brass tubeo of 100 mm outer diameter. The coannular diffusion flame burner which has been used extensively in flames research consisted of an inner brass fuel tube of 10.8 mm inner diameter surrounded by an outer brass tube of 100 mm outer diameter. A schematic of the burner is shown in Figure 2.5. The annular space between the two tubes provided a region for an air coflow. In order to maintain uniform and steady flow conditions at the burner exit, a series of flow restricting devices were placed within the burner. The annular air passage was packed with 3 mm glass beads and a series of fine mesh wire screens. A 25.4 mm thick ceramic honeycomb section (Corning 1.5 mm cell size) was used as the final flow conditioning device in the annular region. The fuel tube extended 4.8 mm above the ceramic honeycomb and it was also filled with 3 mm Pyrex beads to within 50 mm of the top of the burner to condition the fuel flow. A 405 mm long brass cylinder was used to shield the brass cylinder from laboratory air currents. Slots machined in the chimney provided appropriate optical access. Each slot was 6 mm wide and 25 mm high. In order to minimize scattered light, the chimney was painted with flat black paint. The chimney was mounted on a thin ball bearing in such a manner that the chimney can rotate on the burner axis, and translate on the horizontal plane perpendicular to the incident beam, while being centered on the axis of the burner.

In order to facilitate quick and accurate translation, the burner was mounted on a two dimensional stepper motor (Daedal Series 44040 and 44060) controlled translating stage. These stepper motor driven stages provided both horizontal and vertical movements perpendicular to the incident laser beam. Stage positioning could be made with increments of 0.0127 mm in the vertical direction and 0.0254 mm in the horizontal direction, with accuracies of 0.0025 mm and

0.005 mm respectively. The stepper motor stages were controlled using a stepper motor controller (Daedal PC-410). The procedure for locating the absolute position of measurement in the flame was important since extinction and multi-angle scattering measurements are made simultaneously from the same point in the flame. To establish zero position along the vertical direction, a laser attenuation technique was used. In this procedure, the laser extinction set up was employed and the burner was translated until the fuel tube exit interrupted 50 % of the laser beam intensity as determined by a photodiode. Care was taken to ensure that the fuel tube was level so that the laser beam propagated normal to the fuel tube exit. Since the diameter of the laser beam was 0.25 mm. a positioning accuracy of ± 0.125 mm could be achieved. This accuracy was by far the limiting error in determining the vertical position in the flame since the stepper motor system had significantly more positioning accuracy. The absolute horizontal position with respect to the flame centerline was subsequently determined, based on symmetry of the radial profiles, after data had been acquired. This system did not have a translation along the direction of the incident beam. Therefore, to ensure that the laser beam waist was centered along the fuel tube, the position of the focusing lens was adjusted during setup.

Fuel flow rate was determined using a calibrated mass flow meter. The mass flow meter for the fuel used, in this case ethylene, was calibrated using a bubble meter technique where the volumetric displacement of a soap bubble in a glass cylinder was equated to the volumetric gas flow through the mass flow meter. With the calibrated mass flow meter, flow rates could be set to accuracies of better than 2%. Air was measured using a Matheson Instruments model FM-1050 rotameter capable of measuring up to 0.86 liter per second. This rotameter was also calibrated using the bubble meter technique. This system was found to establish flames that remain stable for hours at a time. Fuel used was ethylene of ultrahigh purity of 99.999 %. Air from an in house compressor was used with suitable filters placed in line to remove both particulates and moisture.

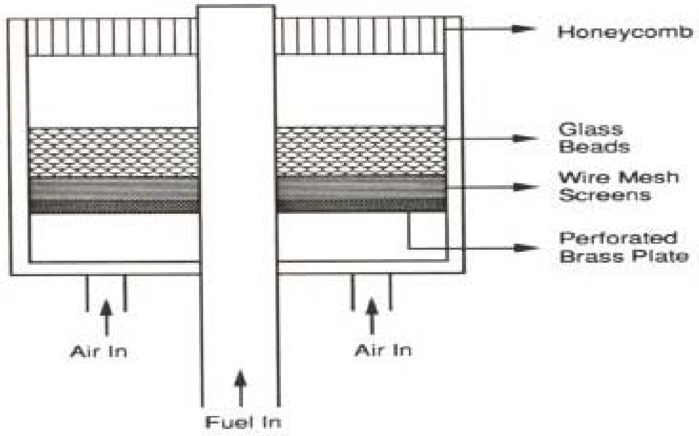

Figure 2.5: Schematic of co-flow diffusion flame burner

2.1.3 <u>TURBULENT SPRAY FLAME</u>

The turbulent spray burner was designed and fabricated as part of the SERDP project. The goal of the design was to create a small spray flame with substantial access to allow optical measurements to be made. The burner was successful in early use, but nozzle fouling problems ultimately made it difficult to get consistent results from the test-to-test. The poor test-to-test repeatability limited the utility of the burner in the overall study so the amount of quantitative data generated in this facility was less than originally anticipated. It did, however, provide important confirmation of the effects of a number of the additives in a spray environment.

The turbulent spray burner consists of two concentric cylindrical stainless steel tubes; see Figure 2.6. Fuel flows through the inner tube while the oxidizer flows through the annulus between the two tubes. The inner tube, through which the liquid fuel flows, has an inner diameter of 6.2mm and an outer diameter of 9.5mm. The outer tube has an outer diameter of 25.4mm, a wall thickness of 0.9mm, and length of 178mm. A peanut nozzle made by Delavan Inc., shown it Figure 2.7, was used for the atomization of the liquid fuel in this study; it has an outside diameter of ¼ inch and provides a nominal 80^o hollow cone spray. The flow number of the nozzle is 0.3. Such a low flow number was required to achieve the small scale flame required for these experiments; however, it ultimately led to the fouling problems. The oxidizer, in this case air, enters into the plenum from the four sides of the chamber simultaneously. From the mixing plenum the air flows through a wire mesh and a honeycomb that produce a nearly uniform velocity profile at the exit plane.

The burner is operated at atmospheric pressure. The tip of the peanut nozzle is centered in a 55° swirl vane assembly (see Figure 2.7), which creates a recirculating flow field, stabilizing the combustion process. The swirler has an OD of 20.3mm and an ID of 9.5mm with 8 vanes and provides a swirl number of 1.1. Liquid fuel is sprayed into this swirling airflow that operates at a sufficiently high velocity that the flow field becomes turbulent. Within this burner, spray processes and turbulent mixing are important in addition to chemical kinetics and molecular diffusion. Some of the fuel droplets evaporate, and the vapor mixes with air to form premixed combustion regions. However, some of the fuel does not completely evaporate or mix with enough air for premixed combustion, so diffusion flames are also present.

In order to produce a steady flame and for the safety consideration, it is necessary to shield the flame with a chimney from laboratory air currents and put it under an exhausted vent. A 12 inch high by 9 inch wide high temperature window was mounted in three of four walls of the square chimney. Two windows are for optical access of the excitation laser source; and the other one, which is 90 degree to the laser beam path, is for the LII signal measurement. The hole, which is covered with a shutter on the wall without the window, is used for ignition. The flames were ignited by means of a torch. Once the flame was lit, the torch was withdrawn.

The fuels and air supply systems are shown in Figure 2.8. The fuels with and without the additive are stored in two different tanks. The fuel flow can be easily switched by a three way valve connecting the fuel tanks. The fuels are pumped into the nozzle by pressurizing them with argon. The fuel and the airflow rates are controlled by pressure regulator and rotameters, which were calibrated with Ventura and standard gas meters. The pressure dispensing fuel tank has a capacity of three gallons. Its maximum working pressure is 150 psig. At the experimental conditions in this work, the pressure, which is directly related to the fuel flow rate, is around 100 psig. The fuel is conditioned by a 15 micron filter. In addition, the whole fuel line can be purged by pure argon. A switch value was installed in the argon supply line to permit easy switching between pressurizing the fuel and purging the fuel line.

Laser-induced incandescence (LII) was the major diagnostic used in the turbulent spreay flame to image the soot in the flames. Due to the turbulent nature of the flame, it was important to be able to get high time resolution so LII was well suited to the experiment. The LII signal was produced by excitation with a Continuum Nd:YAG Q Switched pulse laser, Surelite NY 6 1. It is equipped with a second harmonic generator to produce the 532 nm laser output. The output beam has a diameter of approximately 8 mm with measured divergence of 0.5 mrad. It can produce approximately Gaussian spatial energy profiles, with pulse duration of 5 7 ns FWHM. The Q Switch delay and the flash lamp voltage were held constant during the experiments. As discussed above, LII signals were observed through a narrow band pass filter, 430 ± 10 nm, so the interference from any fluorescence present could be minimized. A schematic of the optical layout is shown in Figure 2.9. A dichroic mirror directed the incident laser through a cylindrical lens and into the combustor. A cylindrical lens was used to form the 270 mJ per pulse laser beam into a 7.5 inch wide sheet. Since LII is generated for a short time after a cloud of soot is irradiated with an intense laser light, synchronization between the laser pulse and the collection of the LII signal is required. An oscilloscope was used to detect the laser output and set the gate the camera.

2-D images were collected at 90° to the propagation direction of the laser beam using a Princeton Instruments intensified charge-coupled device (ICCD) camera with a UV Nikkor f/4.5 105 mm. lens. This orientation reduced the Rayleigh scattering present in the signal. Camera timing was provided by a Princeton Instruments Controller (Model ST 138), and gating was controlled by a Princeton Instruments pulse generator (Model FG 100). The detection system was triggered from a synchronous trigger output of the laser. A standard timing configuration was used to obtain imaging rates as high as 10 Hz. The ICCD camera has a 14 bit resolution. The LII signal dependence on particle size and the soot volume fraction is valid only if the soot approaches its maximum temperature when LII signal is at its peak valve. Therefore, a narrow gate width of 50 ns, and a short delay of 10 ns were used in this experiment. The prism, focus lens, and sheet forming lenses were set on an adjustable scaled stage, so the laser sheet could be adjusted along the height direction of the flame. The ICCD camera also sat on an adjustable scaled stage. In order to obtain satisfactory spatial resolution, multiple fields of view were required to capture the full flame height, which was facilitated by movement of the optics and camera.

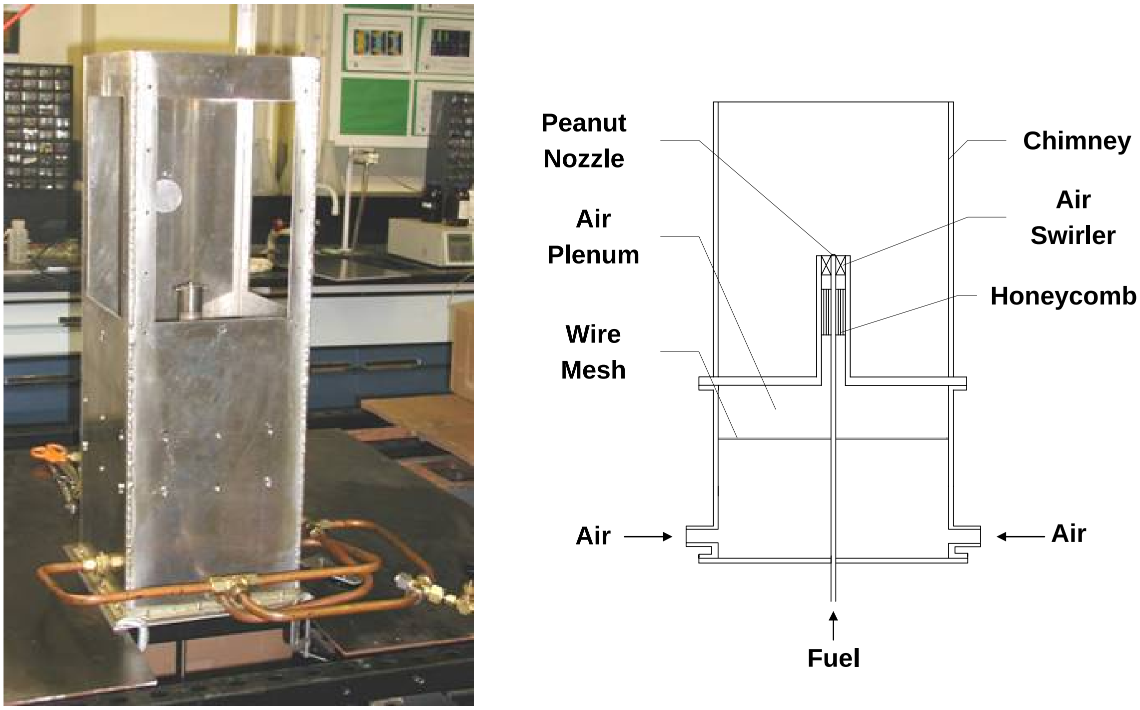

Figure 2.6: Image and schematic of turbulent spray burner

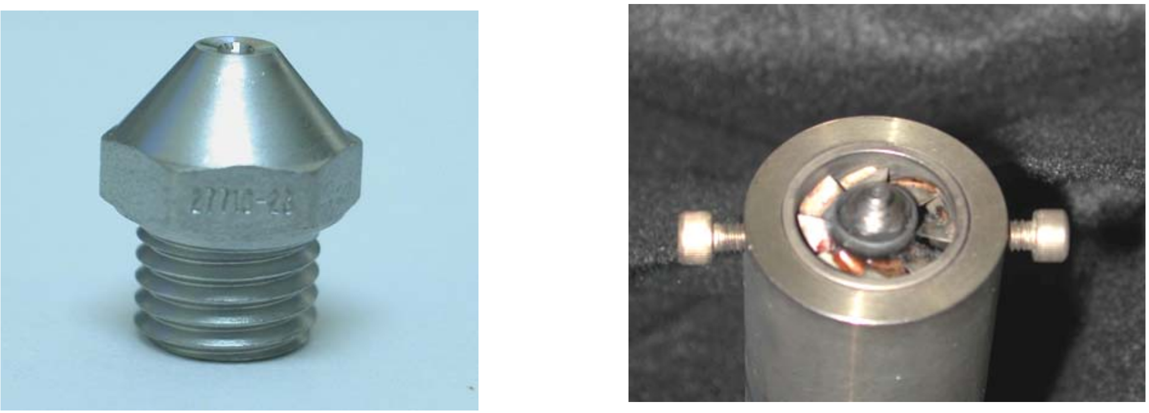

Figure 2.7: Nozzle and air swirler for turbulent spray burner

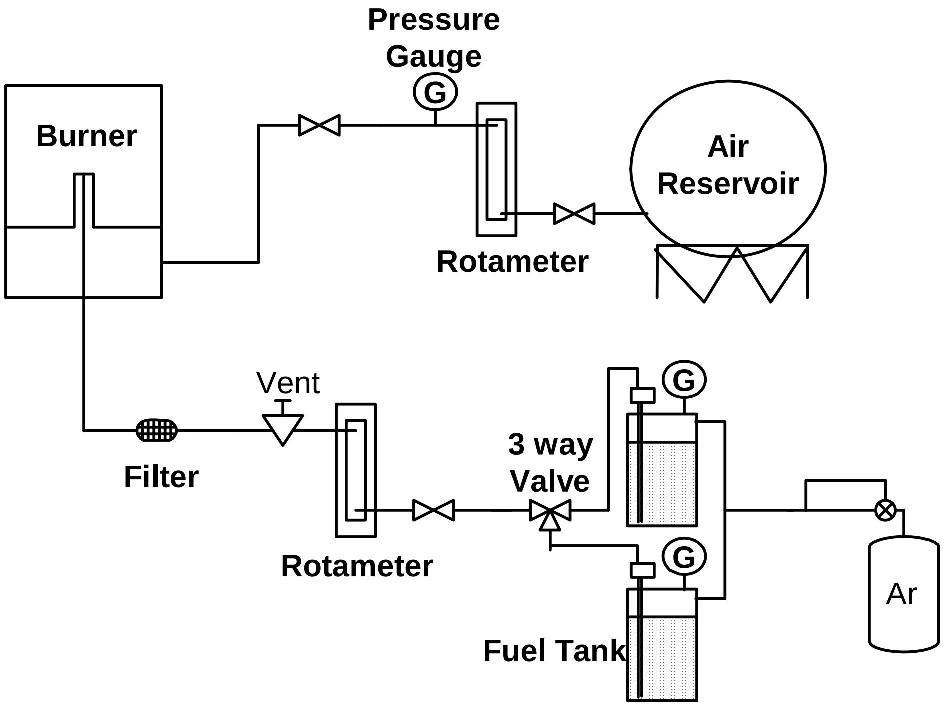

Figure 2.8: Flow control system for turbulent spray burner

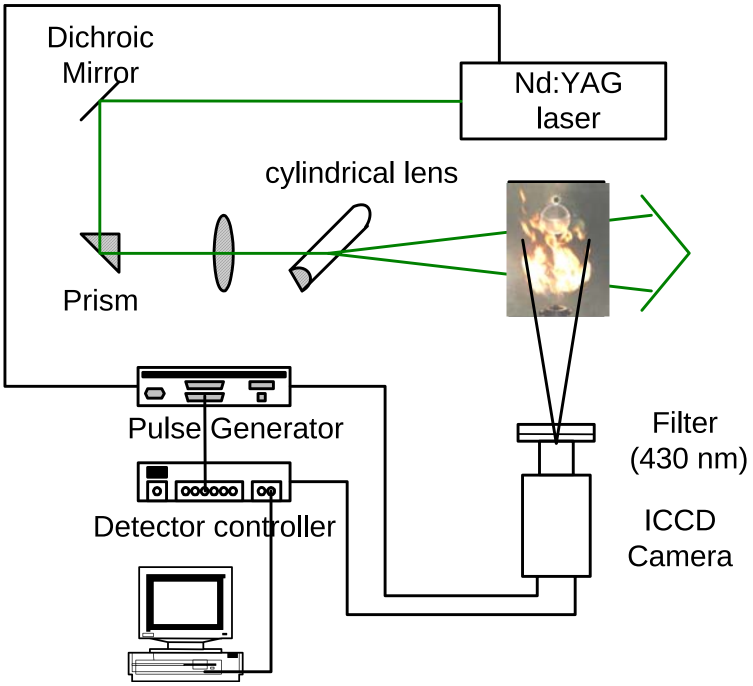

Figure 2.9: Optical set-up for LII measurements for turbulent spray flame

2.1.4 HIGH PRESSURE TURBULENT REACTOR

A schematic diagram of the high pressure turbulent reactor is shown in Figure 2.10. The combustion chamber itself consists of several modular stainless steel sections that allow changes in the overall length of the combustion chamber as well as the location of any of the measurement devices or diagnostics being used. The first chamber section from the dump plane is optically accessible through a 2mm thick, 104mm long cylindrical quartz window. The outer portion of this section consists of a stainless steel housing containing three separate quartz windows providing optical access to the internal quartz combustion chamber. The following two stainless steel sections are 114mm and 51mm long. The 51mm long section contains two flat horizontally opposed quartz windows which are 13mm in diameter, through which extinction measurements can be made. These windows are cooled and kept clean by flowing nitrogen gas over them at a flow rate of approximately one gram per second.

The last section is a 30° converging exit nozzle which is 39mm long with an exit diameter of 10mm. Note that all stainless steel sections have an internal coating of cubic zirconium oxide to provide a heat resistive barrier which protects the stainless steel from the intense heat produced by the combustion. After the exit nozzle, the combustion products enter the inner portion of a heat exchanger, consisting of two concentric stainless steel pipes, before exhausting into the chimney. The liquid fuel supply tube consists of two concentric stainless steel tubes in which the inner tube is used for liquid fuel and the outer tube is used for cooling air. An annular flow of cooling air, about 8% of the total combustion air flow, is maintained along the outside of the inner tube in order to prevent fuel from vaporizing prior to reaching the injector tip. The cooling air is injected radially outward into the mainstream combustion air immediately downstream from the swirler.

In the present study a Delavan pressure atomizer, commonly referred to as a peanut injector, was used as the fuel injector. The peanut injector has a flow number of 2.0 and a full spray angle of 90° with a hollow cone spray pattern. The flow number of a liquid injector indicates the effective flow area of a pressure atomizer. The flow number is expressed as the ratio of the nozzle throughput to the square root of the fuel-injection pressure differential and liquid density. The fuel additives were introduced into the liquid fuel line using a high accuracy syringe pump

(0.5% of set point) located approximately 4.7m upstream of the liquid fuel injector. Uniform mixing of the additive and the fuel was obtained using an inline static mixer.

Temperatures and pressures at various locations along the rig were monitored by using K-type thermocouples and Setra pressure transducers. In addition, the upstream pressure of the fuel injector was closely monitored to ensure that the fuel injector did not become clogged. High-frequency piezoelectric pressure transducers were also used to monitor pressure fluctuations of the chamber pressure to ascertain that the combustor was operating under stable conditions throughout the experiment.

Due to the complexity of flow conditions in this apparatus, repeatable experimental data was very hard to achieve on a regular basis and great emphasis had to be taken to assure proper operating conditions were repeatably achieved. For example, self-sustained pressure oscillations can lead to a significant decrease in the amount of soot formed due to an enhanced burning rate, leading to more intense mixing processes and shorter residence times. Thus, a number of preliminary test experiments were conducted to determine a range of optimum flow conditions needed to produce a steady flame over a wide range of fuel consumption rates.

Soot volume fractions were determined by laser extinction measurements using an argon-ion laser operating at 514.5nm. The collimated laser beam was mechanically chopped at approximately 1000Hz and then directed through the two nitrogen purged quartz windows located 248mm downstream from the dump plane. A portion of the incident laser beam, I, passed through the combustion chamber and its intensity was monitored using a silicon photodiode. The output signal was amplified by a Stanford Research System Model SR530 lock-in amplifier. Concurrently, the incident laser beam intensity, I_o, was also monitored by a separate silicon photodiode and lock-in amplifier. The signal output from the lock-in amplifiers was collected at a sampling rate of three Hz using an A to D system, and processed with LabView software. The soot volume fraction was estimated using Rayleigh's approximation with the refractive index of soot particles taken as 1.57-0.56i at 514.5nm, and a known path length of 45mm. All measurements were made over a 30 second time duration. In the case of the atmospheric turbulent spray burner, measurements were made at a location of 178mm above the injector tip. The soot volume fractions were estimated using flame width measurements obtained from digital camera images of the flame.

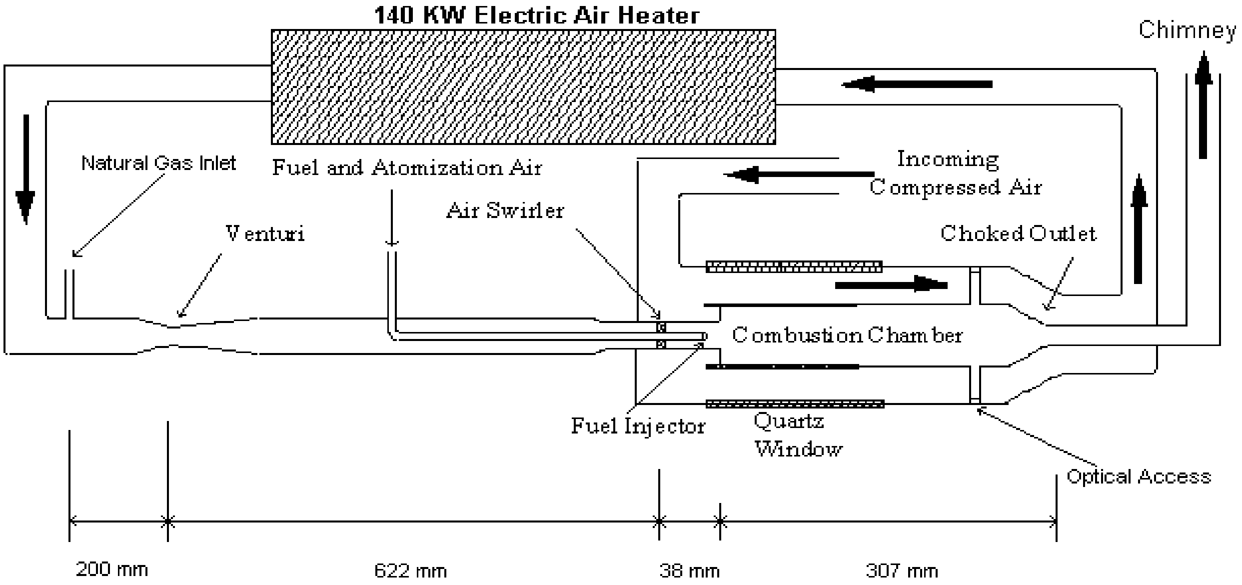

Figure 2.10. Schematic diagram of high pressure turbulent reactor

2.2. COMPUTATIONAL

2.2.1 *CHEMKIN*

For the premixed flames, simulations were conducted with the PREMIX subroutine of the CHEMKIN package. Although the program is capable of computing the temperature profile, experimentally measured temperature profiles were used for all simulations. Use of a measured temperature profile in the computations eliminates the need to model heat loss in the energy equation, which significantly reduces computing time. Mass flow rate through the burner, gas composition, pressure, temperature and estimated initial solution profile were used as input.

Additional analysis of the results was conducted using a post-processor, XSenkplot, which determines the production and destruction fluxes of a given species for all reactions involving that species, and an in-house post-post processor that uses the output from XSenkplot. The reaction flux analysis was used to identify primary reaction sequences leading to PAH formation and growth pathways. XSenkplot, developed at NIST, is an interactive graphics postprocessor for numerical simulations of chemical kinetics to post-process the CHEMKIN family software package. It displays mole fractions, production and destruction rates of species, and reaction pathways as a function of time or distance. The inputs for this software are binary files of the chemical mechanism and a solution file describing time or space dependent species concentrations in reacting systems. An important feature of XSenkplot is calculation of the net rate profiles of production of species of interest, which facilitates the development of a fundamental understanding of coupled chemically reacting systems by providing the ability to probe the impact of process parameters and reaction mechanisms. Utilizing XSenkplot, reaction pathways from initial hydrocarbon fuel to soot precursors, production and destruction rate of each species, and net production profile of PAH species were obtained as a function of height above the burner surface.

2.2.2 REACTION MECHANISMS

In collaboration with the NIST SERDP team a number of mechanisms were created during this program that were required for simulation of the effects of the additives. Two kinetic mechanisms for ethylene were used in this study. The first was the detailed reaction set provided by M. Frenklach (Frenklach and Wang, 1990) and modified at PSU to include oxygenated compounds. It includes species as large as pyrene (a four ring polycyclic aromatic hydrocarbon, $C_{16}H_{10}$, with a mass of 202 atomic mass units, or amu). To these mechanism, species, reactions and related thermodynamics for the ethanol (Marinov, 1998) and DME (Curran et al., 1998) chemistry originally developed at Lawrence Livermore Laboratories were extracted and added to the mechanism.

3. RESULTS

3.1 OXYGENATED ADDITIVES

3.1.1 PREMIXED FLAME

During the initial phase of the program, premixed flame studies were conducted at both Penn State and UTRC. The goal of the parallel experiments was to cross-check the results to ensure accuracy and consistency of the results. When the work shifted to liquid fuels, this parallel effort was deemed to be too costly in time and resources to be continued no work with liquid fuels in the premixed flame was conducted at Penn State. The premixed flame studies of oxygenated additives at Penn State included ethanol and dimethyl ether (DME). The DME study was done to investigate the effect of structure on the effectiveness of an additive. Both sets of results are reported here. In each case modeling was used to understand the trends observed, so modeling results are also presented.

In the ethylene studies, flames with equivalence ratios of Φ=2.34, and Φ=2.64 were studied to facilitate comparison to past work on ethylene flames. Two oxygen concentrations, 5 and 10 wt% in the ethylene/additive mixture, were studied. 5 wt% oxygen requires a 14.4 % mass fraction of ethanol in the fuel stream, and 10 wt% requires approximately twice this amount. When the ethanol was introduced into the fuel line, the ethylene flow rate was reduced in appropriate proportion in order to keep the total carbon flow rate constant. Because of the fuel and oxygenate selected, the equivalence ratio was not affected by the introduction of the ethanol so adjustment of the air flow rate was not required to keep the equivalence ratio constant. The mass fluxes used in the experiments are summarized in Table 3-1; the designation UHP denotes ultra-high purity and implies that the ethylene was 99.9% pure.

The fluorescence spectra for flames with Φ=2.34 and Φ=2.64 as a function of height above the burner are presented in Figure 3.1. The fluorescence spectra show a broadband in the UV range centered around 340nm where the intensities are almost constant along the flame height up to 10mm; this band was used as an indicator of small aromatic species with one or two rings based on the work of Beretta *et al*. (1992) Another broadband peak in the visible range around 540nm is observed for flame height above 6 mm, for which the intensity increases strongly as a function of flame height. This band was used as a qualitative measure of PAH species with three or more rings. The spectral features observed are in good agreement with those of Sgro *et al*. (2001) in a similar ethylene/air flame at equivalence ratio of 2.31.

Figure 3.2 shows small aromatic species, large PAH, and soot volume fraction at Φ=2.34 and Φ=2.64 for the ethylene-air flames. Along the height above the burner surface, small PAH is first observed. The onset of small PAH appears to be located around 1mm above the burner. After a sharp increase, the signal from the small aromatic species reaches a local maximum at the flame height of about 3mm. At about 10mm, the signal again rises, perhaps due to the growth of two-ring species. Large PAH begin to rise after the small aromatic species and continue to increase over the distance of measurement. Soot volume fraction follows the trends of the large PAH. However, the onset of soot is about 5mm above the burner, which is much later than the onset of small aromatic species and large PAH. The clear time sequence among the development of small aromatic species, large PAH and soot is consistent with the expectations based on current theories of soot formation.

A comparison of the soot measurements to the work of Xu *et al*. (1997) is presented in Figure 3.3. Below the flame height of 10mm, the data show a good consistency with those of Xu *et al*, measured using both optical and gravimetric methods. The configuration of the stagnation plate used in this study is different than that used by Xu *et al.*, which may account for a large portion of the differences observed. In the present study, 100-mm-diameter, 10-mm-thick aluminum plate was placed 36 mm above the burner surface to stabilize the flame. Xu *et al.* also used a stagnation plate in their experiments, but their plate was made of stainless steel and had a 30-mm-diameter hole in the center and was place 32mm above the burner surface. In the present study, a stagnation plate identical to that of Xu *et al.* was used. However, after one hour of testing, soot accumulated around the hole and filled it in so that the size of the hole was less than 10 mm. The filling of the hole caused measurable changes in the soot profile within the flame. In order to avoid these changes, a solid aluminum plate was used. Another contributing factor is that the total flow rate at Φ=2.64 was reduced to 80% used by Xu *et al.*, in order to obtain a stable flame condition with the solid stagnation plate, so the Φ=2.64 case had a lower mass flux than the corresponding flame of Xu *et al.* At Φ=2.34, the flow rates are exactly the same, much smaller differences are observed.

The effects of ethanol addition on aromatic species and soot are presented in Figure 3.4 and changes in maximum values relative to the baseline are presented in Table 3-2. For both equivalence ratios the addition of ethanol has a greater effect on large PAH and soot than on the smaller aromatic species. Also the data indicate that the effect of ethanol addition is greater at Φ=2.34 than at Φ=2.64.

The temperature profiles, which were obtained for use in the modeling studies, are presented in Figure 3.5. Each set of measurements was made at least twice in separate experiments; the repeatability of the temperature measurement was typically within ±20K. Temperatures are higher at ϕ=2.34 as expected; however, the trend of increasing maximum temperature with the addition of the ethanol was counter to expectations. Such a trend is also reported by Inal and Senkan (2002); they do not, however, offer an explanation for it. A possible explanation for the unexpected trend in the flame temperature observed in the present study is that the addition of ethanol lowers the flame speed of the mixture. The lower flame speed causes the flame to stabilize further from the burner, lowering heat loss and counterbalancing the effect of ethanol on the adiabatic flame temperature.

Figure 3.6 presents comparisons between the model and experiment for small aromatic species, large PAH, and soot for the ethylene-air flames. The model results track the experimental trends with equivalence ratio reasonably well for small aromatic species and large PAH, but the trends in soot are not captured as well. For small aromatic species, the modeling results for the dominant one and two ring species, benzene and naphthalene, were combined. Benzene is much higher in concentration than naphthalene, but the naphthalene will fluoresce more strongly. In order to account for the stronger fluorescence of the naphthalene, its concentration was weighted by a factor of 14, which was determined to be the factor that best matched the Φ=2.34 experimental results. The factor of 14 was used for all other test conditions. The modeling predicts a much larger increase in small aromatic species as equivalence ratio increases than is observed in the experiments. For the large PAH the match between model and experiment is somewhat better; the large PAH predictions were obtained by summing all three-ring and larger aromatic species from the modeling results. The model predicts approximately a factor of two increase in large PAH species as equivalence ratio increases from Φ=2.34 to Φ=2.64, whereas the experiment showed a factor of three increase. The predictions for soot, which are made by post-processing the premixed flame simulation results, show little increase in soot as equivalence ratio increases. The comparison at Φ=2.34 is reasonably good, but the soot model does not predict the increase of nearly a factor of three that occurs in the experiment when equivalence ratio is increased to 2.64.

Figure 3.7 shows the modeling results for all flames studies which are comparable to the experimental data in Figure 4. For small aromatic species and large PAH, the model results capture the general trend that increasing the amount of oxygen leads to greater reductions in aromatic species. Also the magnitudes of the reductions relative to the baseline match the data reasonably well for the aromatic species. The soot predictions for $\Phi=2.34$ are reasonably consistent with the experimental data, although the volume fraction is under-predicted. For $\Phi=2.64$, the comparison of the model and experiment are not good. The model predicts no effect of 5% oxygen at this condition.

The results from the modeling were used to determine the mechanism through which the ethanol leads to a reduction of aromatic species and soot. Since the modeling results matched the experimental results best at an equivalence ratio of 2.34, that condition was used as the basis for the analysis. The first step in the analysis was to track the main reaction pathways for the production of the aromatic species using XSenkplot. The results are summarized in Table 3 which presents the major reaction pathways from the fuel to aromatic species as well as competing oxidation reactions. The primary route for formation of the first aromatic ring is predicted to occur through propargyl recombination; alternative routes involving C_4+C_2 species were not predicted to be important under the conditions of this study. The majority of naphthalene formation occurs through two consecutive Hydrogen-Abstraction-Acetylene-Addition (HACA) reactions via phenylacetylene (C_8H_6); the production via cyclopentadienyl is predicted to be relatively small. The recombination reaction of two cyclopentadienyl radicals (C_5H_5) makes a minor contribution to naphthalene formation at these conditions. A3, phenanthrene, is formed largely by ring-ring condensation reactions as opposed to formation through the HACA growth pathway from naphthalene. The production of pyrene ($C_{16}H_{10}$) is dominated by the HACA mechanism through phenanthryl radical ($C_{14}H_9$), which forms from phenanthrene by H abstraction.

The summary presented in Table 3-3 demonstrates that production of aromatic species is a complex, radical-driven process involving a competition between reactions that oxidize the carbon to CO and CO_2, and reactions that produce aromatic species and their precursors. The quantity of aromatic species formed will be the net result of the competition between the oxidation and aromatic production pathways. The addition of ethanol can change this balance in several ways including effects on temperature, radical concentrations, and the amount of carbon from the ethanol that contributes to aromatic production.

The thermocouple measurements showed that the addition of ethanol led to higher temperatures throughout the regions where aromatic species are formed. Modeling runs were performed for the ethylene/ethanol flames using the same temperature profile as the corresponding ethylene flame to obtain an indication of the effect of temperature on the production of aromatic species. The results, presented in Figure 3-8, show that the temperature is having only a small effect on aromatic species, PAH, and soot over most of the measurement region.

Other researchers have noted that changes in concentrations of radical species such as H, O, and OH can have a significant impact on the competition between oxidation pathways and pathways leading to aromatic species and soot. As an indication of the effect of the addition of ethanol on these key radicals, the changes in the predicted peak mole fractions caused by the addition of ethanol were determined relative to the base fuel. Table 3-4 presents a summary for $\Phi=2.34$ and the two oxygen levels studied based on modeling using the measured temperature profiles and using the temperature profile of the corresponding ethylene flame. The latter data can be used to judge the contributions of the increased temperature to changes in radical concentrations. Comparison of the two sets of results indicates that the temperature is contributing to the changes in radical concentrations. The increases in H atoms appear to be mostly caused by the temperature increase, and for the 5% oxygen case, temperature also appears to be the dominant factor in increasing O and OH. Increasing H will tend to enhance reactions leading to aromatic formation and increasing O and OH will tend to enhance the competing oxidation reactions; therefore, the increases tend to offset each other to some degree. However, it would appear that the increases in the oxidizing radicals may be somewhat more significant than the increase in H and could account for some of the decrease in aromatic species observed in the experiments and the model.

The final effect that is contributing to the reduction of aromatic species is the contribution of ethanol to precursor species. In order to estimate this effect, the pathways through which the ethanol reacts were studied to determine their contributions to precursor species. A simplified reaction map is presented in Figure 3.9 showing its conversion to key products including CO.

Ethanol can decompose via two reactions that break the C-O bond leading to ethylene and methyl, both of which can contribute to the formation of aromatic species. In addition ethanol can undergo hydrogen abstraction at three different sites, leading to three different radical species that subsequently undergo additional reactions eventually leading to precursor species and CO. Methyl undergoes additional reactions that can lead to various precursor species and CO. Due to the strength of the C=O bond, CO will not contribute to the production of aromatic species so any carbon from the ethanol that produces CO is considered to be removed from the reaction pathway leading to aromatic species and soot. This effect has been noted by many others including Curran *et al*. (2001) The carbon flow analysis revealed that only about one-half (54%) of the carbon in ethanol is converted to species that contribute to the production of aromatic species. The majority of this amount (49%) is converted to ethylene or ethane, which is quickly converted to ethylene, and the remainder (5%) contributes to propargyl formation. Thus, about half of that carbon in the ethanol is removed from pathways that can contribute to aromatic species and soot formation.

Table 3-1. Experimental Conditions

Mass flux of premixed ethylene/air flame (mg/s.cm^2)			
Equivalence ratio		2.34	2.64
W/O Additive	Air	6.75	5.31
	ethylene (UHP)	1.07	0.95
5% O in fuel	ethanol	0.16	0.14
	Air	6.75	5.31
	ethylene (UHP)	0.97	0.86
10% O in fuel	ethanol	0.35	0.31
	Air	6.75	5.31
	ethylene (UHP)	0.86	0.76

Table 3-2. Percentage changes in maximum values of aromatic species and soot relative to the baseline by ethanol

Φ	2.34		2.64	
oxygen content	5%	10%	5%	10%
small aromatic species	-10%	-21%	-4%	-17%
large PAH	-18%	-56%	-6%	-28%
Soot	-25%	-44%	-17%	-32%

Table 3-3. Summary of Major Reactions in Pathway from Fuel to PAH at Φ=2.34

Species	Modes	**Main Pathway to Soot Precursor**	**Competing Reaction**
C_2H_4	des	$C_2H_4+H<\rightarrow C_2H_3+H_2$ (49.0%) $C_2H_4+OH<\rightarrow C_2H_3+H_2O$ (13.1%) $C_2H_4+CH_3<\rightarrow C_2H_3+CH_4$ (9.5%) $C_2H_4+O<\rightarrow OH+C_2H_3$ (4.2%)	$C_2H_4+OH<\rightarrow CH_3+CH_2O$ (9.4%) $C_2H_4+O<\rightarrow CH_3+HCO$ (7.8%) $C_2H_4+O<\rightarrow CH_2O+CH_2$ (4.4%)
C_2H_3	prod	$C_2H_4+H<\rightarrow C_2H_3+H_2$ (63.3%) $C_2H_4+OH<\rightarrow C_2H_3+H_2O$ (16.9%) $C_2H_4+CH_3<\rightarrow C_2H_3+CH_4$ (12.2%) $C_2H_4+O<\rightarrow OH+C_2H_3$ (5.4%)	
	des	$C_2H_3<\rightarrow C_2H_2+H$ (71.2%) $C_2H_3+O_2<\rightarrow C_2H_2+HO_2$ (1.0%) $C_2H_3+H<\rightarrow C_2H_2+H_2$ (0.5%)	$C_2H_3+O_2<\rightarrow CH_2O+HCO$ (26.2%)
C_2H_2	prod	$C_2H_3<\rightarrow C_2H_2+H$ (78.9%) $C_3H_2+OH<\rightarrow C_2H_2+HCO$ (9.2%) $C_3H_2+O<\rightarrow C_2H_2+CO$ (2.4%)	
	des	$CH_2+C_2H_2<\rightarrow H_2CCCH+H$ (10.3%) $CH3+C_2H_2<\rightarrow C_3H_4P+H$ (7.6%) $C_3H_4+H<\rightarrow C_2H_2+CH_3$ (2.7%) $C_2H_3<\rightarrow C_2H_2+H$ (2.6%) $HCH+C_2H_2<\rightarrow H_2CCCH+H$ (2.6%)	$C_2H_2+O<\rightarrow HCCO+H$ (48.0%) $C_2H_2+O<\rightarrow HCH+CO$ (11.6%)
H_2CCCH	prod	$CH_2+C_2H_2<\rightarrow H_2CCCH+H$ (38.8%) $C_3H_4P+H<\rightarrow H_2CCCH+H_2$ (27.0%) $C_3H_4+H<\rightarrow H_2CCCH+H_2$ (10.8%) $HCH+C_2H_2<\rightarrow H_2CCCH+H$ (9.7%)	
	des	$H_2CCCH+H<\rightarrow C_3H_2+H_2$ (62.3%)	$H_2CCCH+OH<\rightarrow C_3H_2+H_2O$ (2.3%)
C_6H_6	prod	$2H_2CCCH<\rightarrow C_6H_6$ (66.7%) $C_6H_5+H<\rightarrow C_6H_6$ (20.5%) $OH+C_6H_6<\rightarrow C_6H_5OH+H$ (7.7%)	
	des	$C_6H_6+H<\rightarrow C_6H_5+H_2$ (80.4%) $C_6H_6+OH<\rightarrow C_6H_5+H_2O$ (13.3%)	$C_6H_6+O<\rightarrow C_6H_5O+H$ (2.5%) $OH+C_6H_6<\rightarrow C_6H_5OH+H$ (1.9%)
C_6H_5	prod	$C_6H_6+H<\rightarrow C_6H_5+H_2$ (79.0%) $C_6H_6+OH<\rightarrow C_6H_5+H_2O$ (13.1%)	
	des	$C_6H_5+C_2H_2<\rightarrow C_8H_6+H$ (27.6%)	$C_6H_5+O_2<\rightarrow C_6H_5O+O$ (16.9%)

		C_6H_5+H<→C_6H_6 (23.8%)	C_6H_5+O_2<→$C_6H_4O_2$+H (8.0%)
$C_{10}H_8$	prod	$C_{10}H_8$+H<→$C_{10}H_7$*1+H_2 (45.1%) $C_{10}H_7$*1+H<→$C_{10}H_8$ (25.6%) $C_{10}H_7$*2+H<→$C_{10}H_8$ (13.4%) $C_{10}H_8$+OH<→$C_{10}H_7$*1+H_2O (6.8%) 2C_5H_5<→$C_{10}H_8$+2H (2.4%)	
	des	$C_{10}H_8$+H<→$C_{10}H_7$*2+H_2 (77.5%) $C_{10}H_8$+OH<→$C_{10}H_7$*2+H_2O (10.4%) $C_{10}H_8$+OH<→$C_{10}H_7$*1+H_2O (2.0%) $C_{10}H_8$+H<→$C_{10}H_7$*1+H_2 (0.4%)	$C_{10}H_7$OH-1+H<→$C_{10}H_8$+OH (6.3%)
A_3	prod	C_8H_6+C_6H_5<→A_3+H (50.2%) A_3L<→A_3 (11.8%) A_1C_2H*2+C_6H_6<→A_3+H (9.3%) $C_{12}H_9$+C_2H_2<→A_3+H (8.8%) INDENE*+C_5H_5<→A_3+H_2 (7.0%)	
	des	A_3+H<→A_3*4+H_2 (74.4%) A_3+OH<→A_3*4+H_2O (12.8%)	
PYRENE	prod	A_3*4+C_2H_2<→PYRENE+H (81.6%) A_1C_2H*2+C_8H_6<→PYRENE+H (5.5%) PYRENE*4+H<→PYRENE (4.9%)	
	des	PYRENE+H<→PYRENE*4+H_2 (39.4%) PYRENE+H<→PYRENE*1+H_2 (34.6%) PYRENE+H<→PYRENE*2+H_2 (8.0%)	PYRENE+OH<→PYRENE*4+H_2O (5.8%) PYRENE+OH<→PYRENE*1+H_2O (5.0%)

Table 3-4. Changes in computed peak radical concentrations with addition of ethanol at Φ=2.34.

Temperature Profile	As measured		From Ethylene flame	
Oxygen level	5%	10%	5%	10%
H	4.2%	3.0%	0.6%	0.00%
OH	5.7%	7.4%	1.2%	6.0%
O	2.0%	2.3%	0.2%	2.4%

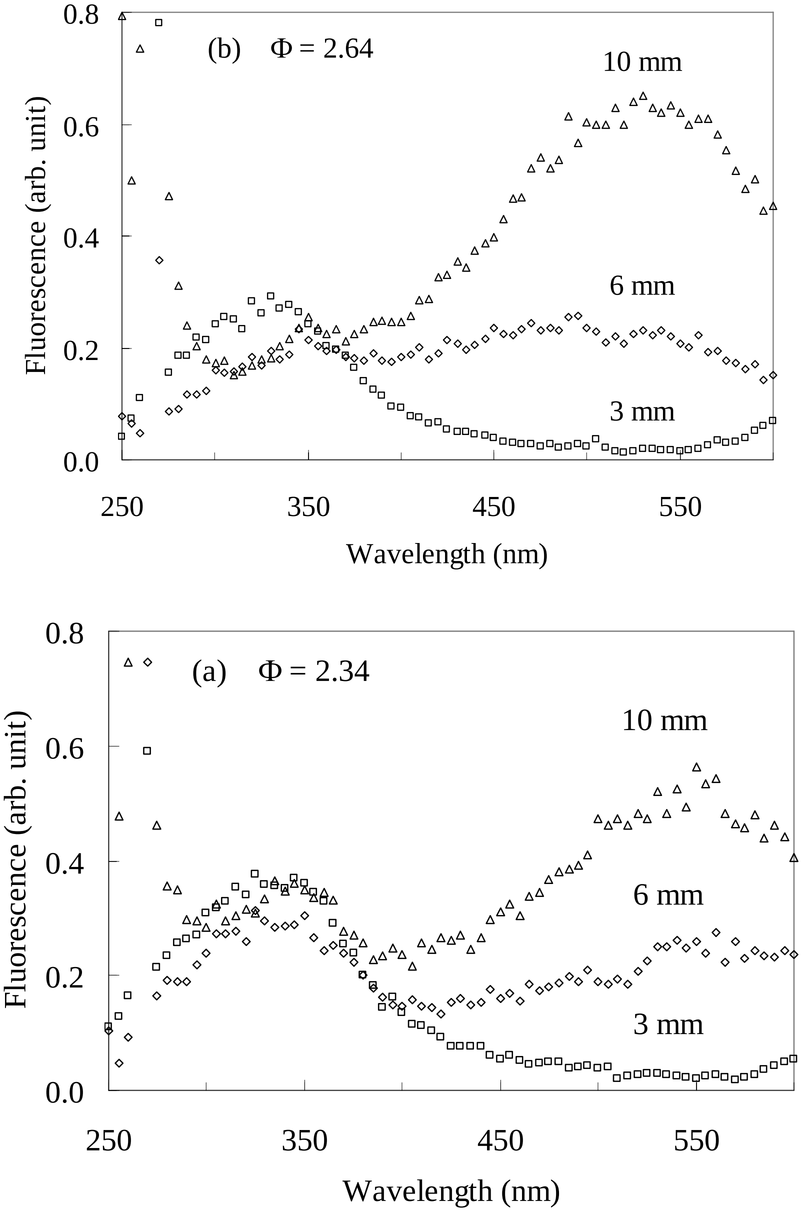

Figure 3.1. Fluorescence spectra. (a) Φ = 2.34; (b) Φ = 2.64

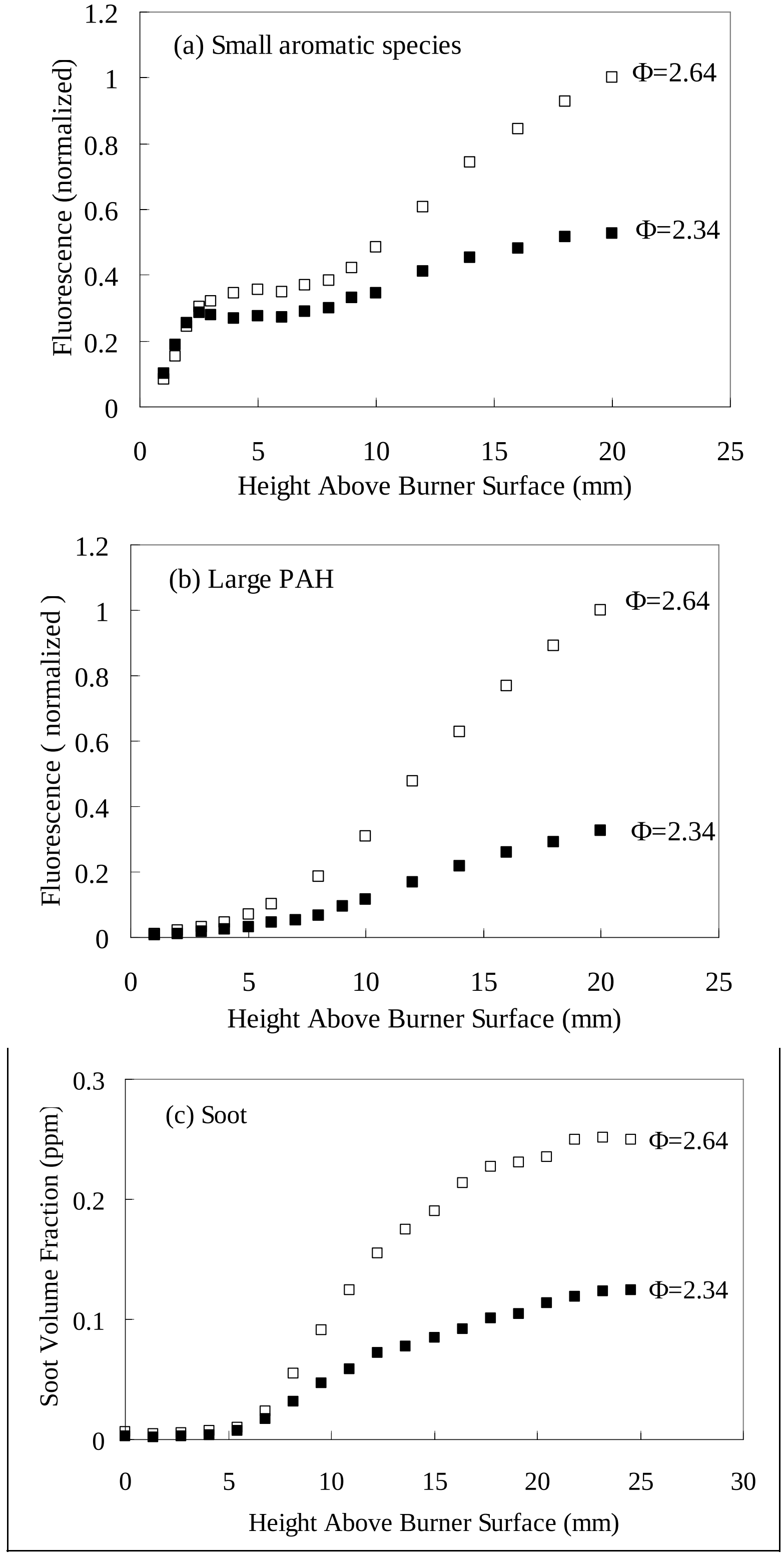

Figure 3.2 (a) Small aromatic species, (b) large PAH, (c) soot for ethylene-air flames. (Note that the PAH data are normalized by the maximum signal observed at Φ=2.64)

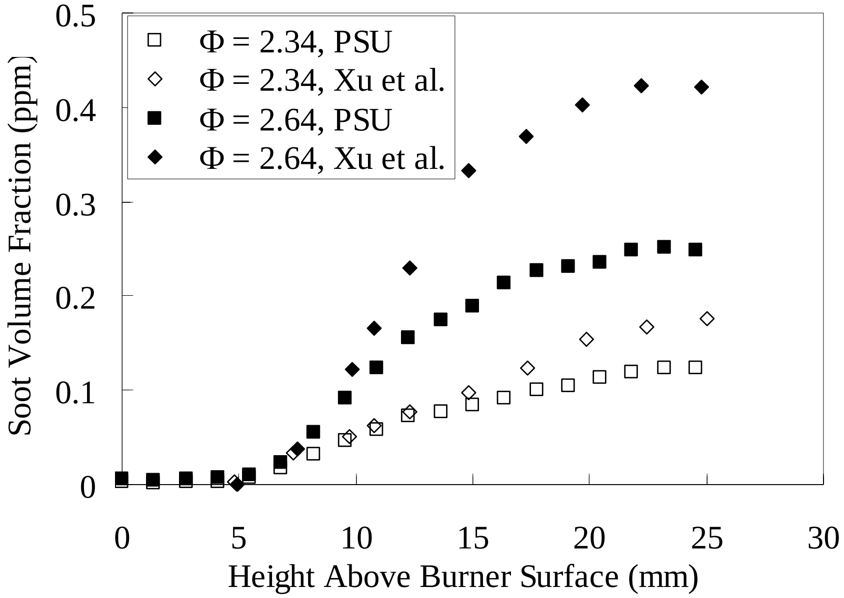

Figure 3.3. Comparison of soot volume fraction measurement results to those of Xu *et al*. [1997]

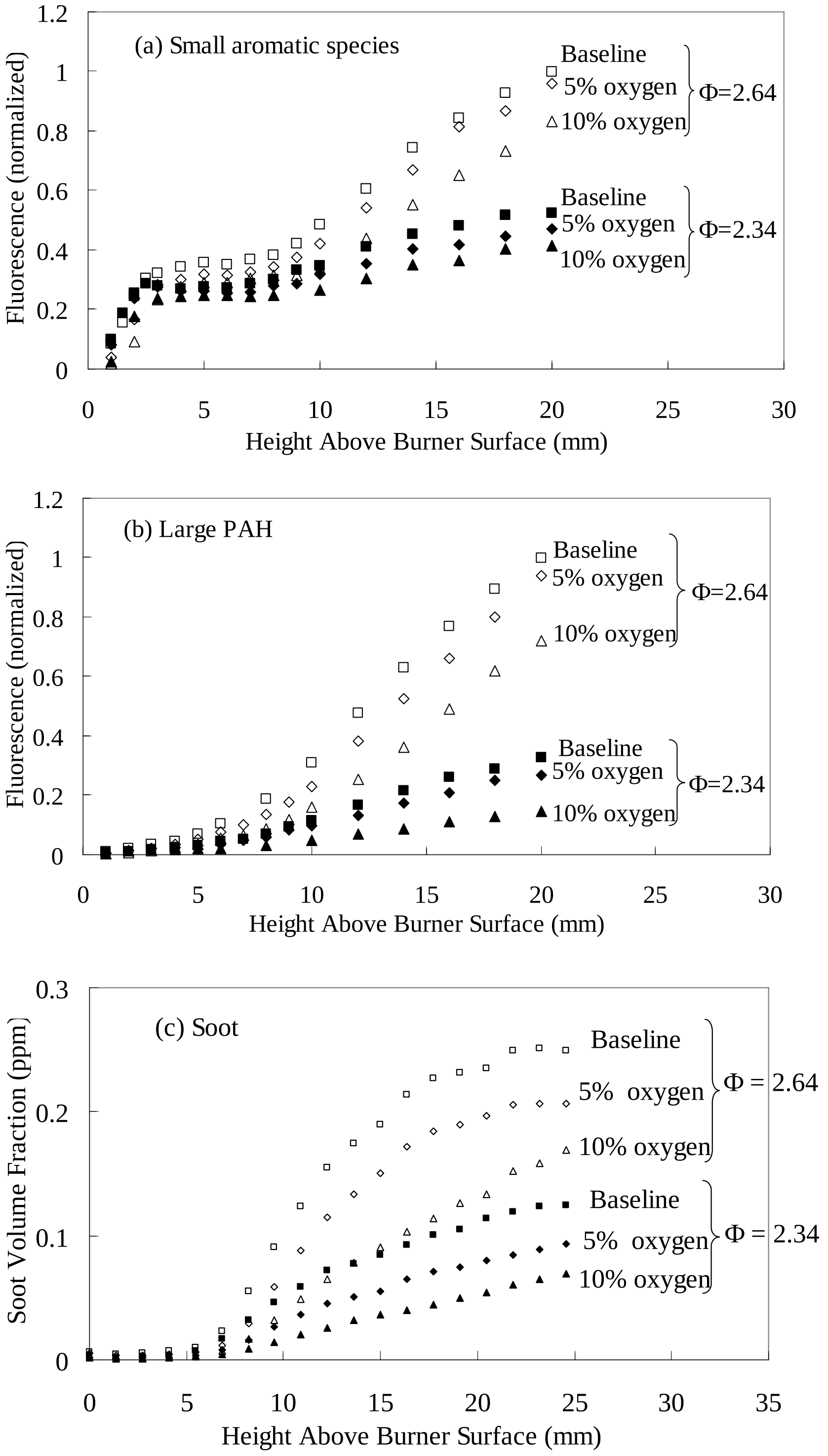

Figure 3.4. Effects of ethanol on (a) small aromatic species, (b) large PAH, and (c) soot for ethylene-air flames. (Note that the PAH data are normalized by the maximum signal observed at ϕ=2.64)

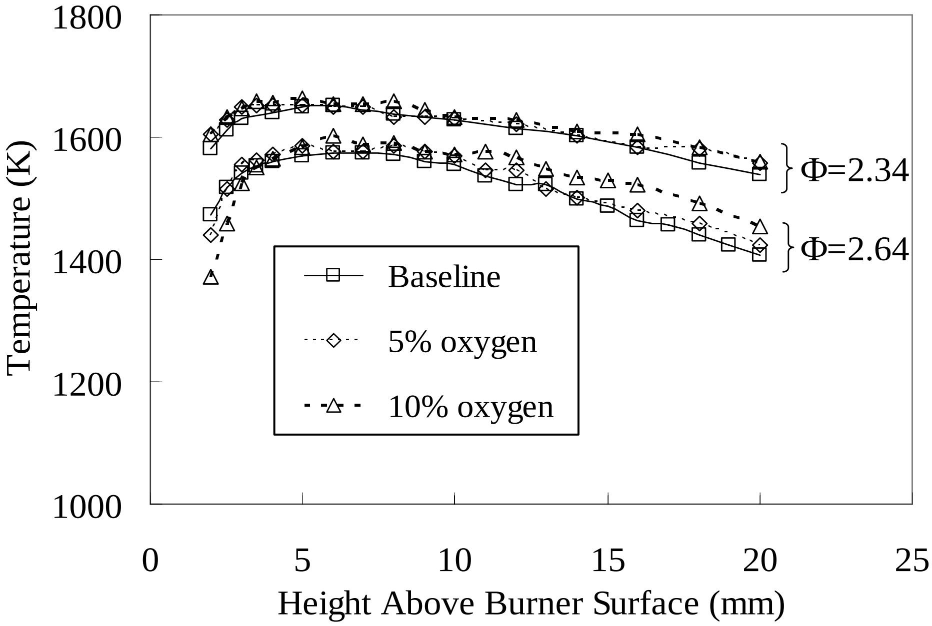

Figure 3.5. Measured flame temperature profiles for Φ = 2.34 and 2.64.

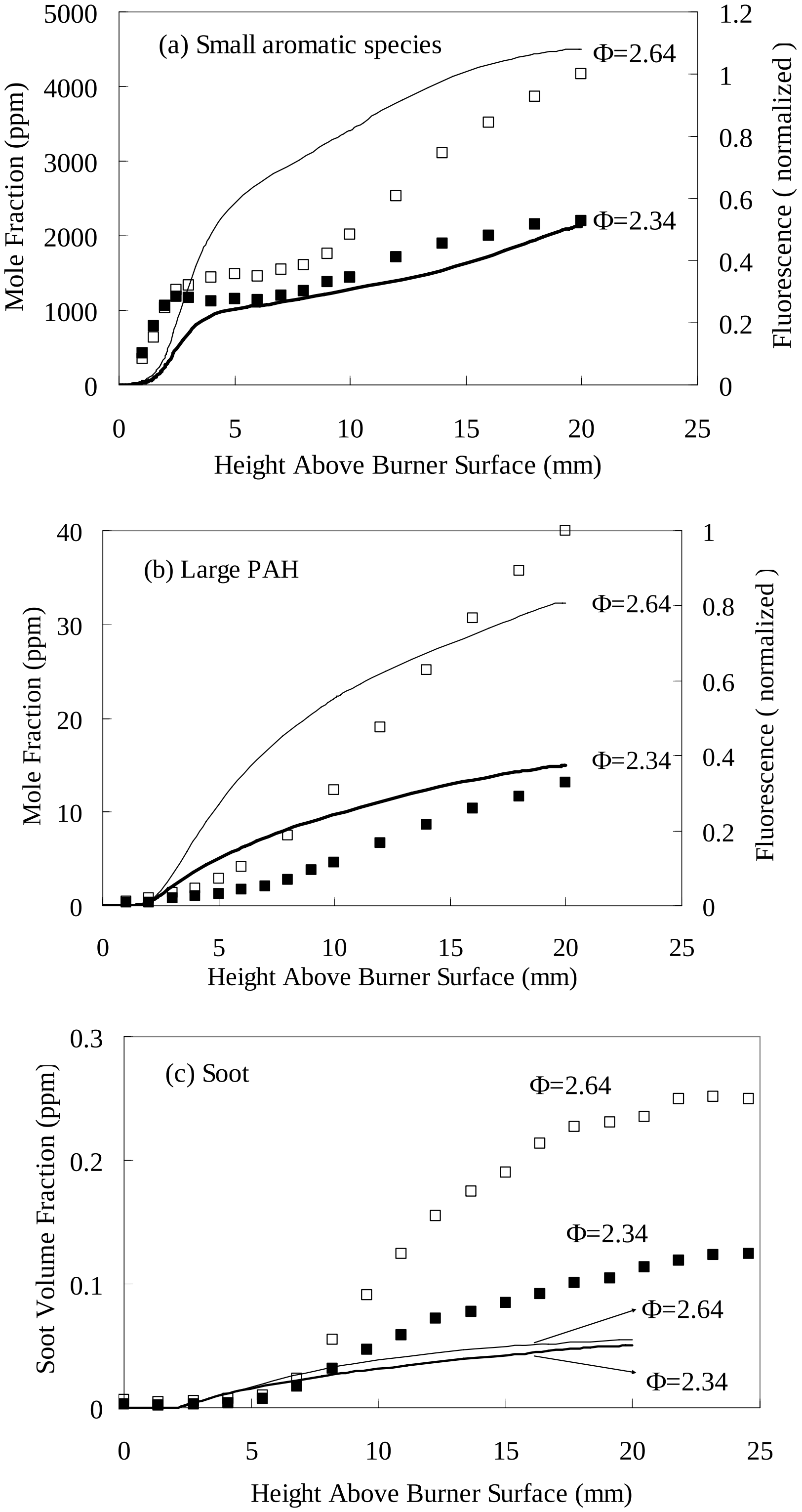

Figure 3.6. Comparison of experiments (square symbols) and model (solid lines) for (a) small aromatic species, (b) large PAH, (c) soot at base flames (LIF data normalized by the maximum signal observed at Φ=2.64)

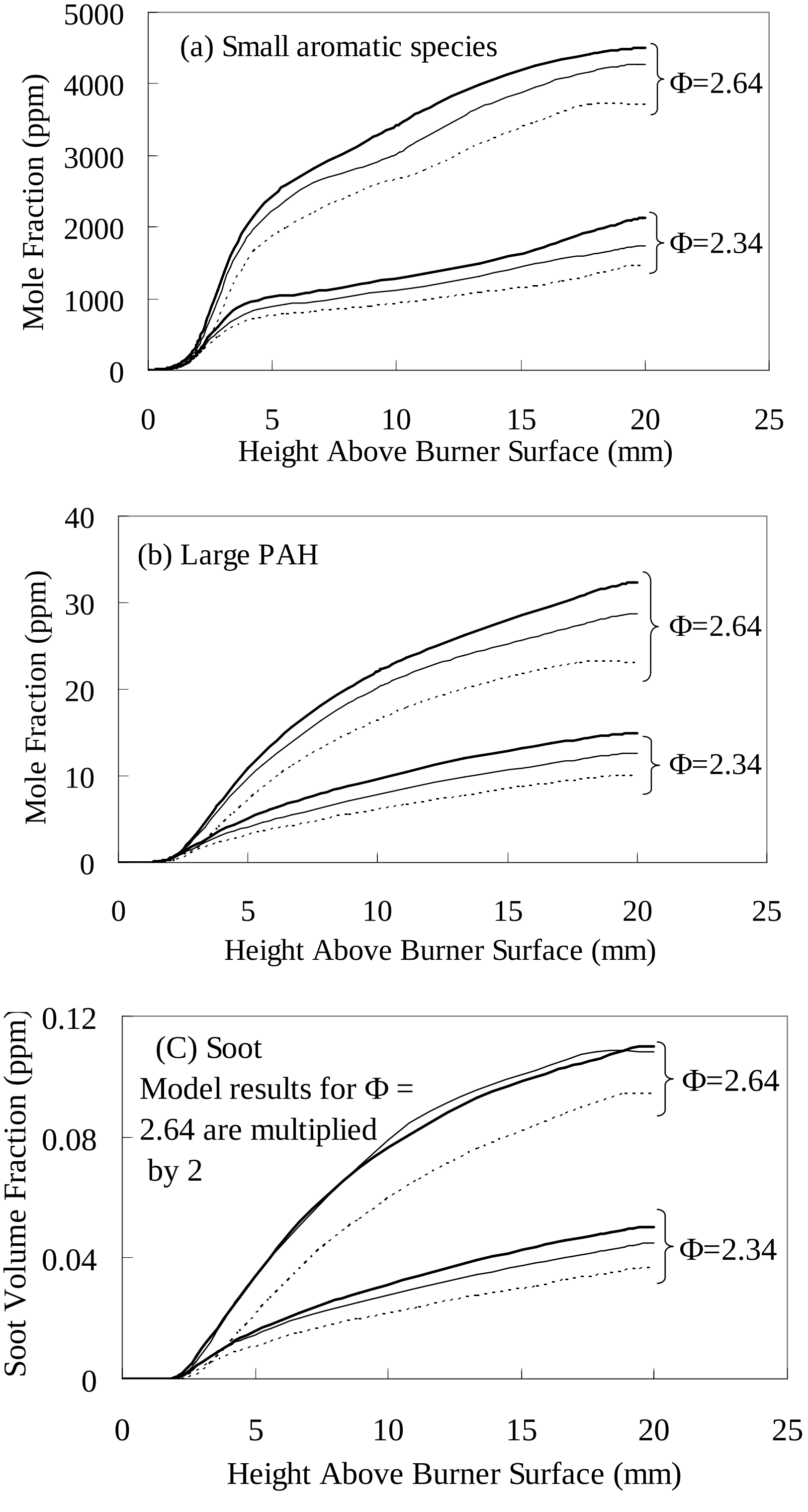

Figure 3.7. Model predictions for effects of ethanol on (a) small aromatic species, (b) large PAH, (c) soot. Thick solid lines represent baseline, thin solid lines represent 5% oxygen and dotted lines represent 10% oxygen. (Note that model predictions of soot for Φ=2.64 case are multiplied by a factor of 2 to separate them from the Φ=2.34 results.)

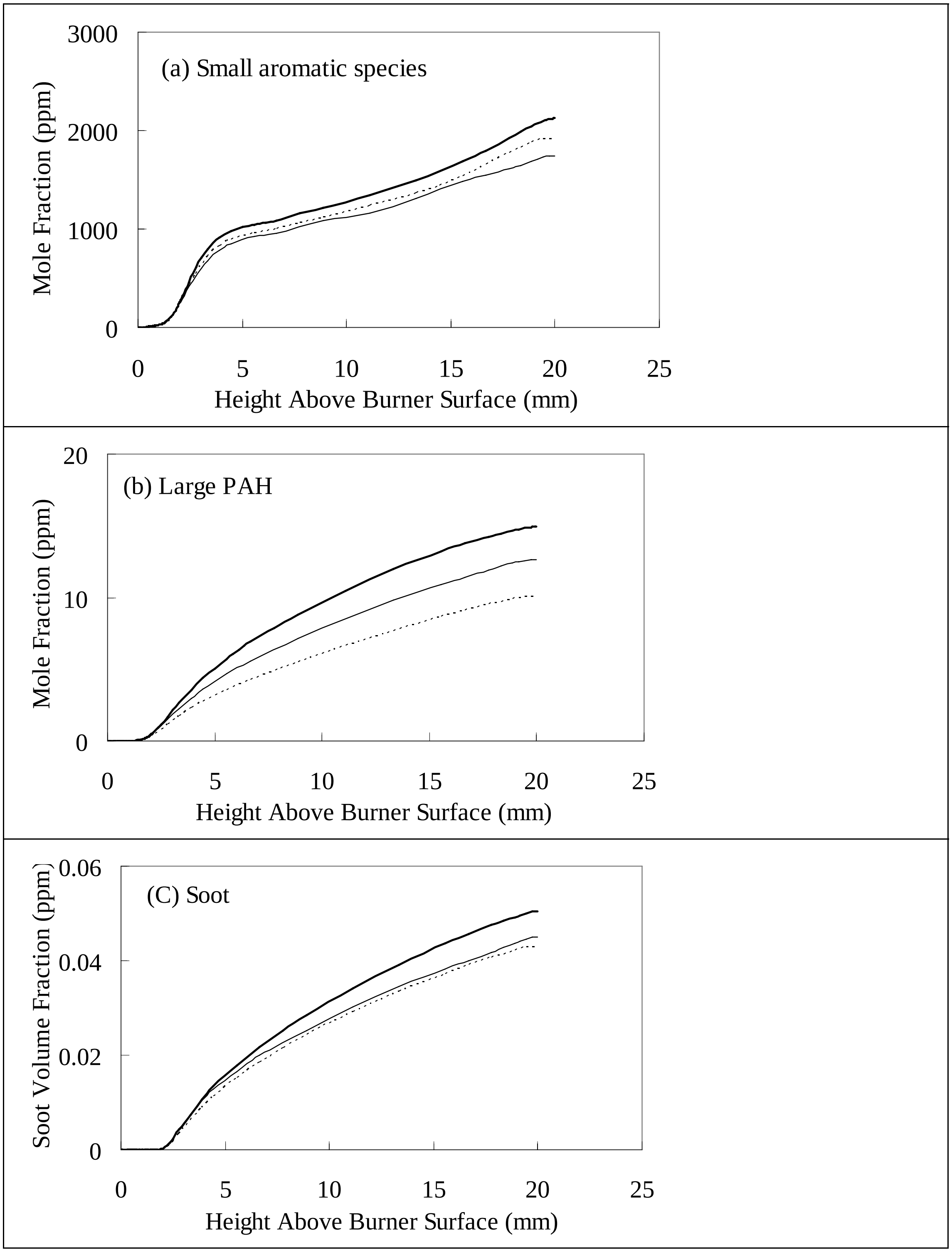

Figure 3.8. Effect of temperature on (a) small aromatic species, (b) large PAH, (c) soot predicted by model at Φ=2.34. (Thick solid lines represent baseline cases; thin solid lines represent 5% oxygen cases with measured temperature profiles, and dashed lines represent 5% oxygen cases with same temperature profiles as the baseline cases.)

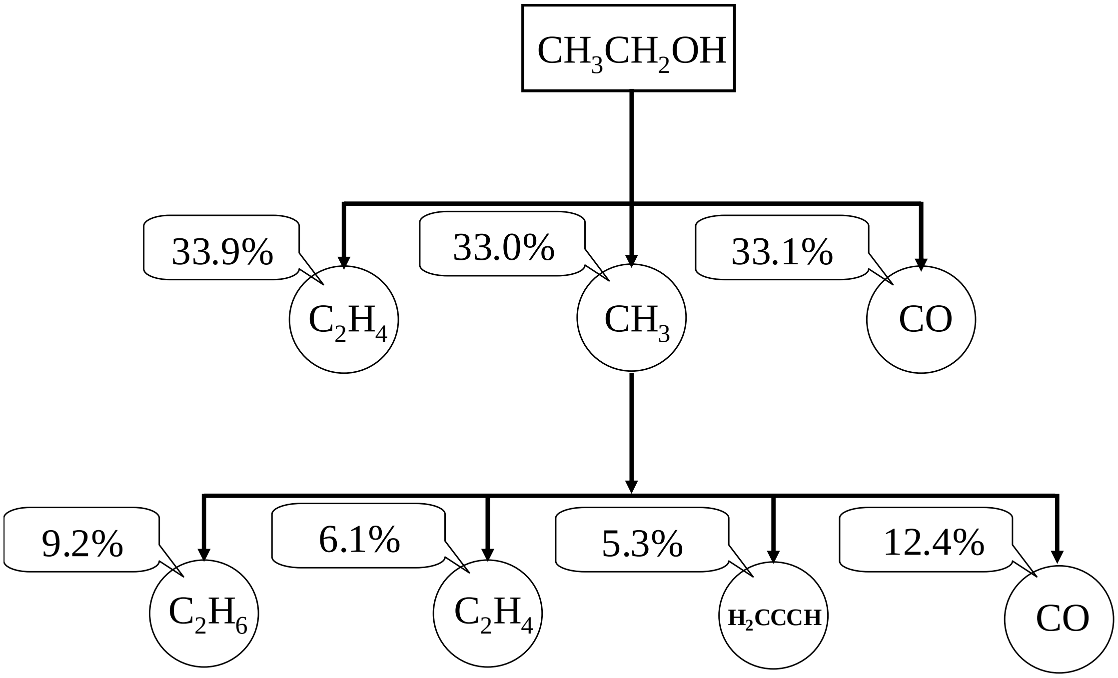

Figure 3.9. Carbon flux diagram for ethanol at Φ=2.34; percentage indicates the fraction of carbon from ethanol passing through the species shown.

Dimethyl Ether

The work with dimethyl ether (DME), which has the same elemental composition as ethanol, was done to investigate the effect of oxygenate structure on soot reduction. The conditions of the study were identical to those used in the ethanol-ethylene experiments as were the experimental and modeling approaches. Therefore only main results will be presented here; complete results are reported in Wu *et al.* (2006).

Flames with Φ=2.34, and Φ=2.64, and two oxygen concentrations, 5 and 10 wt% in the ethylene/additive mixture, were studied. 5 wt% oxygen requires a 14.4 % mass fraction of DME in the fuel stream, and 10 wt% requires approximately twice this amount. When the DME was introduced into the fuel line, the ethylene flow rate was reduced in appropriate proportion in order to keep the total carbon flow rate constant. Because of the fuel and oxygenate selected, the equivalence ratio was not affected by the introduction of the DME so adjustment of the air flow rate was not required to keep the equivalence ratio constant. The mass fluxes used in the experiments are summarized in Table 3-5; the designation UHP denotes ultra-high purity and implies that the ethylene was 99.9% pure.

Table 3-6 presents a summary of the reductions in peak soot and PAH levels achieved through the addition of DME to the flames. Comparison of these reductions from the addition of ethanol under similar experimental conditions indicates that the DME is somewhat more effective than ethanol in reducing soot at Φ=2.34 and about equivalent to it at Φ=2.64. Modeling indicated that the effects of DME are similar to those identified for ethanol. The main effect of structure that was identified that can account for the somewhat greater effectiveness of DME is that it has no decomposition path that involves the formation of C_2-species that can contribute directly to the formation of soot precursors. On the other hand, ethanol can undergo unimolecular decomposition to form an ethyl radical that can contribute to soot formation. Details of these differences are discussed in Song, *et al.* (2003).

Table 3-5. Experimental Conditions

Mass flux of premixed ethylene/air flame (mg/s.cm^2)			
Equivalence ratio		2.34	2.64
W/O Additive	air	6.75	5.31
	ethylene (UHP)	1.07	0.95
5% O in fuel	DME	0.16	0.14
	air	6.75	5.31
	ethylene (UHP)	0.97	0.86
10% O in fuel	DME	0.35	0.31
	air	6.75	5.31
	ethylene (UHP)	0.86	0.76

Table 3-6. Percentage changes in maximum values of aromatic species and soot relative to the baseline by DME

Φ	2.34		2.64	
oxygen content	5%	10%	5%	10%
small aromatic species	-19%	-49%	-6%	-19%
large PAH	-34%	-70%	-20%	-35%
soot	-34%	-62%	-13%	-32%

3.1.2 <u>TURBULENT SPRAY FLAME</u>

Heptane (99%) was the fuel for the initial studies in the turbulent spray flame. Several equivalence ratios were tested initially with ethanol as the additive, but most of them led to weak LII signals. After increasing the equivalence ratio to 2.76, relatively strong signals and good repeatability were achieved. The experimental conditions of the study are listed in Table 3-7. The amount of ethanol was set so that it introduced 5% oxygen by weight into the fuel (with fuel defined as heptane and ethanol) while keeping the total carbon flow and the equivalence ratio constant.

In the swirler-stabilized flame, Reynolds Number, along with the swirl number, is also a key factor for the onset of the vortex breakdown phenomenon (Syred and Beer, 1974). The significant dimensions of the flame will be determined primarily by the airflow pattern for the pressure jet flames. Therefore, the Reynolds Number for the airflow is an important indicator of the onset of turbulence in the flame. This study used the Reynolds Number based on the cold air at the outlet of the swirler. The values of the Reynolds Number and the parameters, which determined the Reynolds Number, are listed in Table 3-8. Although the value is not in the highly turbulent range, the flame in this study is no doubt in the turbulent regime. Observations of the flame itself verified that it was indeed turbulent.

Examples of averaged and single shot LII images from this study are shown in Figure 3.10 and Figure 3.11, respectively. The regions of highest average LII signals are located towards the sides of the image, which is consistent with the flow field created by the swirler and hollow-cone spray formed by the nozzle. The asymmetry of the soot field is due somewhat to the fact that the beam is attenuated by the soot field, but there also appears to be some asymmetry inherent to the nozzle itself. The single shot image displays the intermittent eddy like soot structure whose location, shape, and volume fraction change with time in the turbulent flow.

Due to the low signal to noise ratio of LII in this experiments, it was important to remove the background noise before analyzing data. The first noise source, and the simplest form of noise to correct, is the background flame luminosity. It can be directly subtracted from data collected in a manner identical to that used for collecting the LII signal but with the laser beam blocked prior to entering the flame. 400 accumulated images of the flame without laser illumination present were averaged to obtain the background signal. With the laser beam passing through the flame, the averages were taken over a series of 800 laser shots for pure heptane as the base fuel. A comparison of LII images before and after the background correction is shown in Figure 3.12.

It was found that the portions of the two images that overlapped would often have different average intensity, even though nothing was changed but the camera position. The main reason is that individual pixels of the ICCD camera have variable responses to a given light intensity, as demonstrated by Quay (1998) using a similar camera. For quantitative LII measurements, it is desirable to be able to correct variation in pixel response. There are three options available for making the correction; the first is to take the average for the overlapped area, leaving the other part of images unchanged. The second method is to set one image as the base, add or subtract the average intensity difference of the two overlapping regions from the other images. The third method is similar to the second one except using a ratio of the average intensity of the two overlapping regions to adjust for the different intensity. It was found after testing, the third method had the best result when the image taken at the lower camera position was used as the base for correction.

ICCD camera has a field of view that is substantially smaller than the spray flame. Because the view field of ICCD camera cannot cover the entire spray and flame region, two overlapped images were collected at two heights, giving measured signals from the tip of the nozzle to a height of 6.3 inches above the nozzle, as shown in Figure 3.13.

The effects of ethanol on soot formation in the heptane spray flame were determined based on averages of 800 images for the two fields of view shown in Figure 3.13. Corrections were made for background luminosity and pixel-to-pixel variation as discussed above. The results were used to plot average intensity across the image as a function of height above the nozzle and the result is presented in Figure 3.14. The data in the figure has been filtered so show the overall trends more clearly. Overall the addition of ethanol to heptane reduced soot in the order of 30%. Similar to the results obtained for the addition of ethanol to ethylene in the premixed flame.

Table 3-7: Experimental Conditions for Heptane-ethanol study in Turbulent Spray Burner

Base Fuel Formulation	Heptane
Additive	Ethanol
Base Fuel Supply (g/s)	0.32
Fuel with additive Supply (g/s)	0.34
Air Supply (g/s)	1.76
Equivalence Ratio	2.76

Table 3-8: Cold-flow Reynolds for air flow

Effective diameter	m	0.0176
Average exit velocity	m/s	6.13
Kinematic viscosity	MI/S	1.57e-5
Reynolds Number		6872

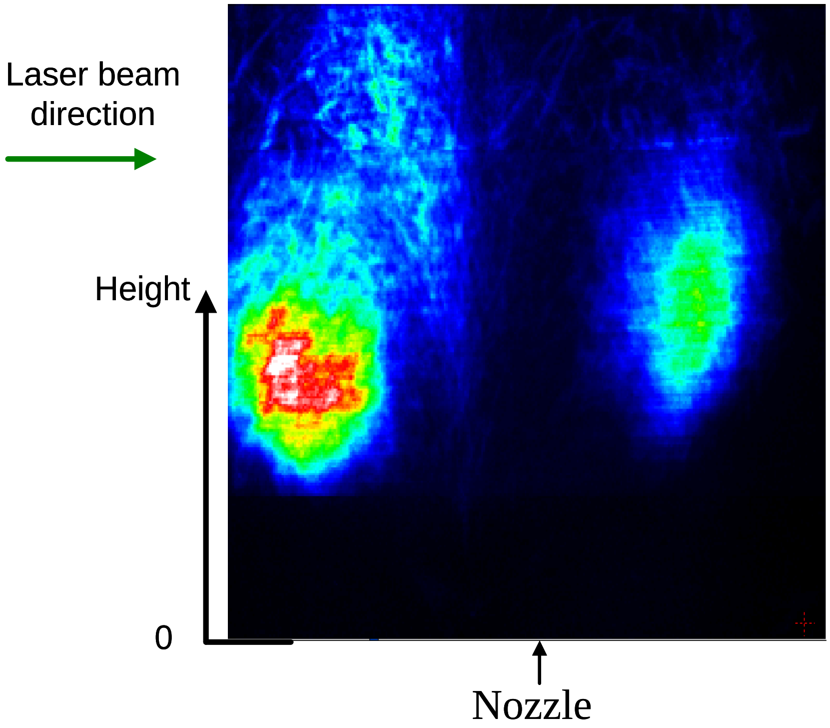

Figure 3.10. Sample averaged LII image from heptane spray flame

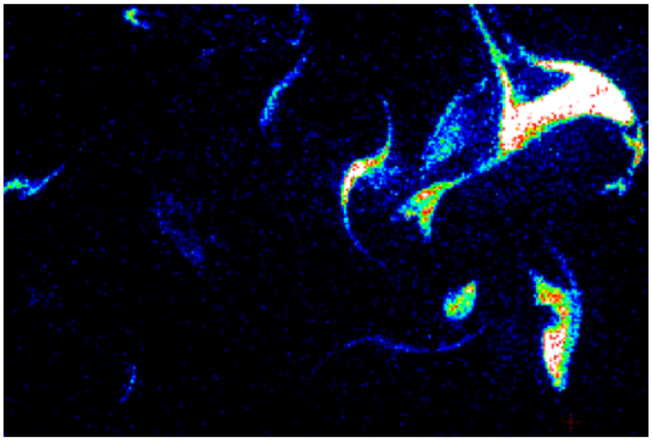

Figure 3.11. Sample single shot LII image from heptane spray flame

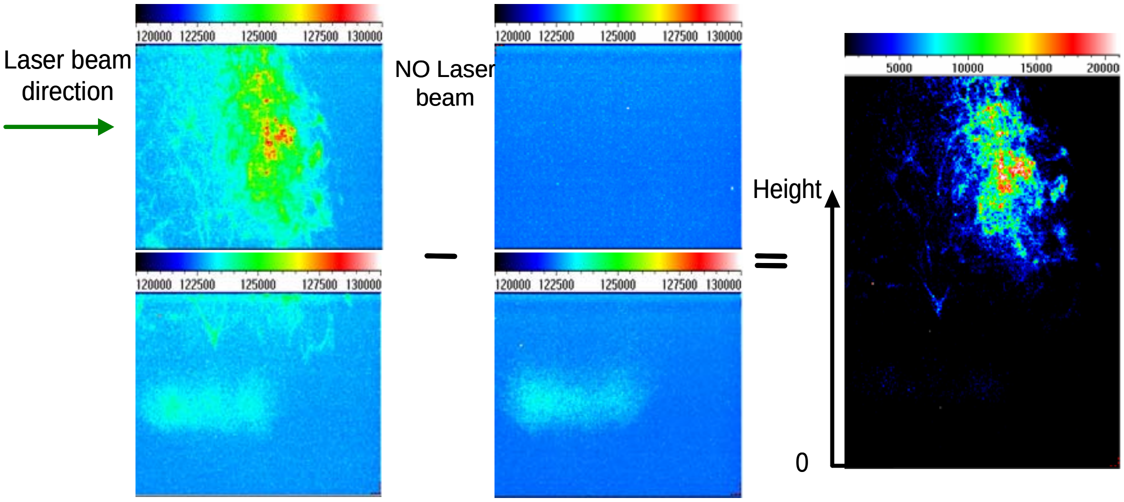

Figure 3.12. Comparison of LII images before and after background correction

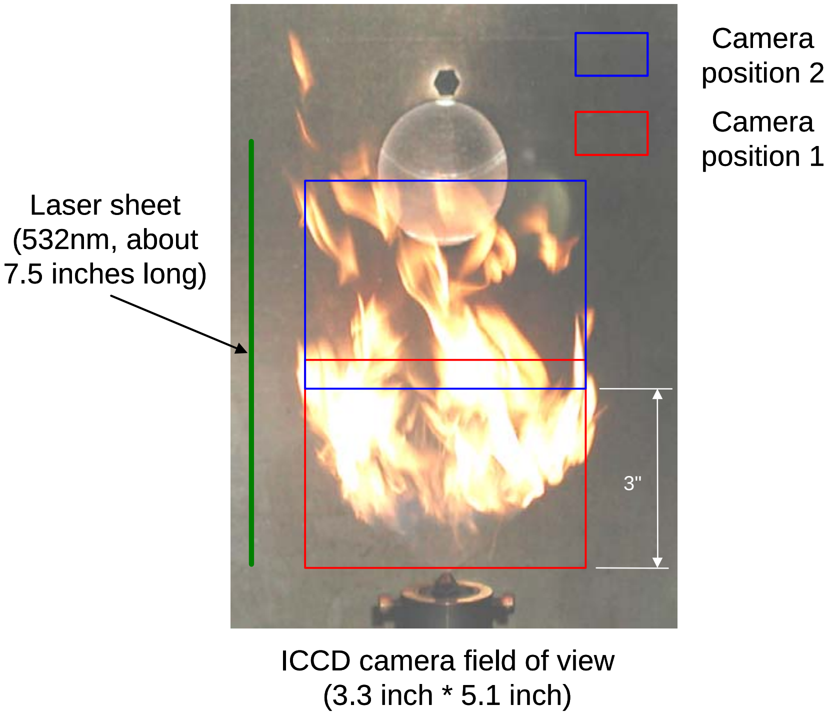

Figure 3.13. Overlapping of fields of view required to cover full extent of the flame

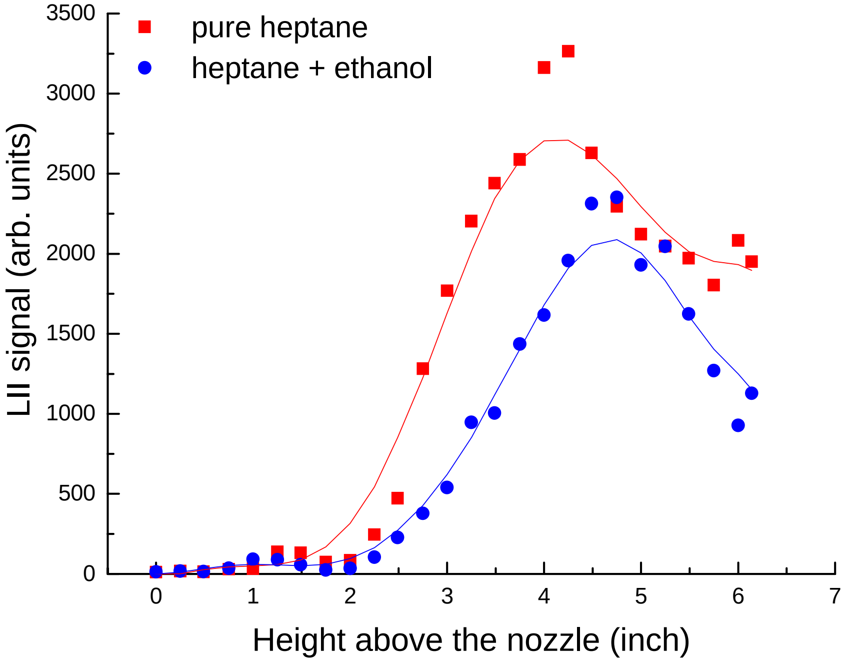

Figure 3.14. Effects of ethanol addition on soot

3.1.3 HIGH PRESSURE TURBULENT REACTOR

All tests with oxygenated additives in the high pressure turbulent combustor were run with JP8 as the fuel; a major consideration being its reasonable cost compared to the heptane/toluene blend. The air flow for the tests was 32 gm/s and the equivalence ratio was Φ=1.3. The inlet air temperature was 550K and the chamber pressure was 0.5 MPa. Three oxygenated additives were investigated ethanol, cyclohexanone, and methanol. The cyclohexanone was an oxygenate contained in a commercial additive that was also studied in the program. This additive also contained nitro-alkanes for which the results appear in the next section. Methanol was studied as a comparison to the ethanol since it had shown good potential to reduce soot in prior work with sooting diffusion flames. For cyclohexanone and ethanol a range of concentration was investigated up to 10% by volume. Methanol was only studied at the highest concentration.

Figure 3.15 presents a summary of the test results on soot volume fraction versus additive concentration. Ethanol was added to the fuel at concentrations ranging from approximately 2.5%

to 10% by volume of the JP-8. The extent of decrease in soot formation was found to increase with increase in additive concentration. The effect on soot formation ranged from about a 10% decrease at a concentration of 2.5% by volume to approximately 40% reduction in soot with an additive concentration of 10% by volume. The dump combustor adds spray processes, turbulence and elevated pressure to the phenomena that can affect the soot formation process beyond pure kinetics and molecular diffusion that are the key processes for the simpler devices used in this study. The fact that the magnitude of reduction is similar among all of these experiments suggests that the same processes are effecting the soot reduction, namely chemical kinetic processes.

Although trends similar to ethanol were observed for cyclohexanone, the soot reduction effect was considerably lesser than both ethanol and methanol. The soot reduction ranged from approximately 10% at an additive concentration of about 2.5% by volume of JP-8 to about 20% reduction in soot at an additive concentration of 10% by volume of JP-8. Thus the cyclohexanone appears to be less effective than the ethanol. Methanol was added to JP-8 in concentrations of approximately 10% by volume of JP-8 fuel; a decrease of approximately 50% was observed, larger than for ethanol. However, comparison on the basis of volume of additive is misleading since at the same volume percent the cyclohexanone will provide less oxygen in the fuel than ethanol and methanol will provide greater oxygen level in the fuel. Figure 3.16 presents the same results plotted against the percent oxygen in the fuel. It shows that the three oxygenates fall on essentially the same curve of soot reduction, which indicates that the soot reduction in each case is largely being driven by the same phenomena.

The levels of soot reduction are similar to those obtained in all of the other devices used in this program will suggests that the same mechanism is dominant in the reducting of soot. The one process common to all devices studied is chemical kinetics, so the results suggest that kinetic processes are dominating the reduction in soot.

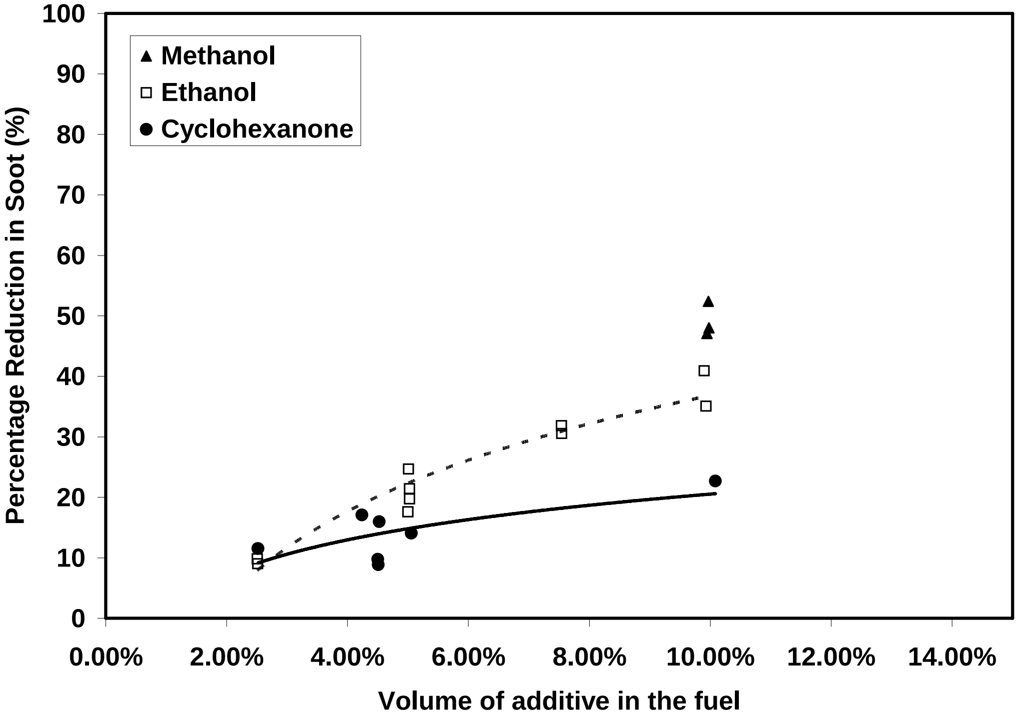

Figure 3.15: Effect of Oxygenated Additives on soot formation with JP-8

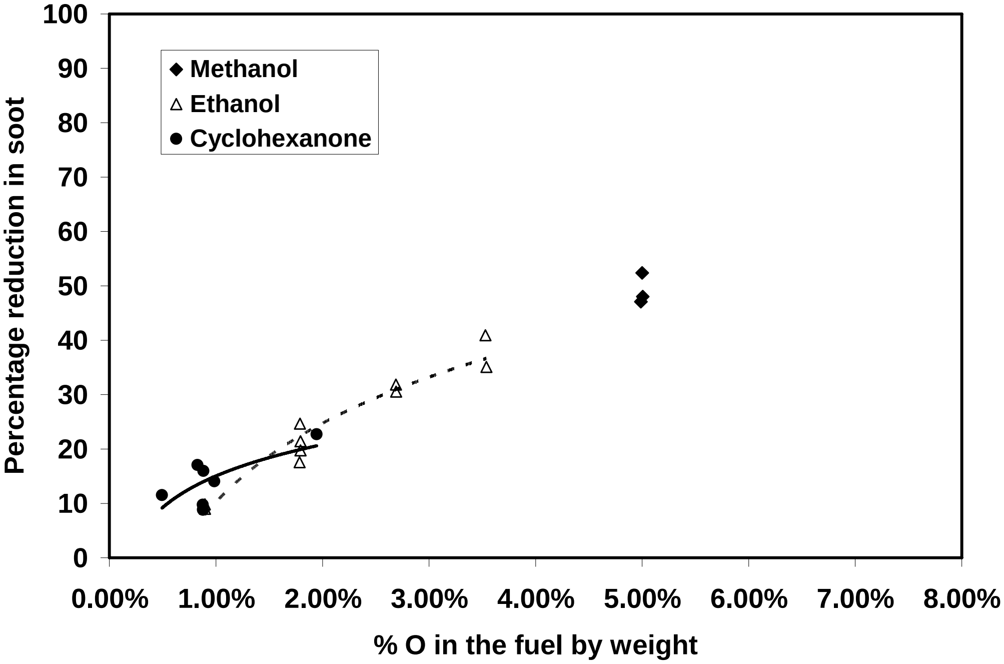

Figure 3.16: Effect of Oxygenated Additives on soot formation with JP-8

3.2 NITRO-ALKANES

3.2.1 TURBULENT SPRAY FLAME

A mixture of 20% toluene/80% heptane was used as the base fuel for these experiments to better approximate the composition of JP-8 relative to pure heptane. Due to the greater tendency to soot of this fuel compared to pure heptane, the experiments were run at a leaner equivalence ratio of 2.37 versus 2.76 for heptane. The air flow rate was the same as that for the heptane-ethanol experiments so the cold-flow Reynolds number was identical for the two sets of tests. The commercial additive was added at 5% by volume. At the time of the initial experiments with the commercial additive, its chemical constituents and properties were not available. Therefore, the fuel flow rates with and without the commercial additive were not corrected, but adopted the same value. The experimental conditions of the study are listed in Table 3-9.

Subsequent to the initial experiments with the commercial additive, its basic composition was determined and the main components with a potential to reduce soot were identified as cyclohexanone, nitromethane, nitroethane, and nitropropane. These components were run individually in the turbulent spray flame to determine their effectiveness in reducing soot under conditions similar to those listed in Table 3-9. Nitromethane was not run in these experiments because of the possibility that it could explode upon compression. The tests were done at two levels of oxygen addition, 2% and 4% of the fuel by mass.

The commercial additive showed very interesting time dependent behavior in these experiments. After it was first introduced the amount of soot decreased slowly to a steady state level and when the additive was removed the soot increased slowly toward the initial baseline level. This behavior is illustrated in Figure 3.17. A number of experiments were run to determine the cause of this slow time response. Unfortunately, difficulty getting good repeatability in these experiments due to nozzle fouling made it impossible to determine the cause of the time dependent behavior.

Data to determine the effect of the additive on soot were collected during the steady periods of behavior. 300 shot averages were used and the results were background corrected and also corrected for pixel-to-pixel variation. Figure 3.18 presents a plot of the average LII intensity for the flame with and without the commercial additive. The results for the commercial additive show that it has a greater effectiveness than ethanol. Soot yields decreased by about 40%, even though its volume fraction is significantly less than that used for ethanol.

Following this work, experiments to test other possible additives were initiated. Figure 3.19 presents summaries of the effect of the nitroethane and nitropropane on soot formation in the turbulent spray flame. The effectiveness of ethanol and cyclohexanone are also presented for comparison purposes. The nitro-alkanes are both more effective than ethanol at equivalent oxygen levels, and the cyclohexanone leads to soot reductions on the order of those for ethanol.

Table 3-9: Experimental Conditions for Heptane/Toluene Fuel and Commercial Additive

Base Fuel Formulation	80% Heptane, 20% Toluene by volume
Additive	Commercial Additive
Base Fuel Supply (g/s)	0.28
Fuel with additive Supply (g/s)	0.28
Air Supply (g/s)	1.76
Equivalence Ratio for baseline test	2.37

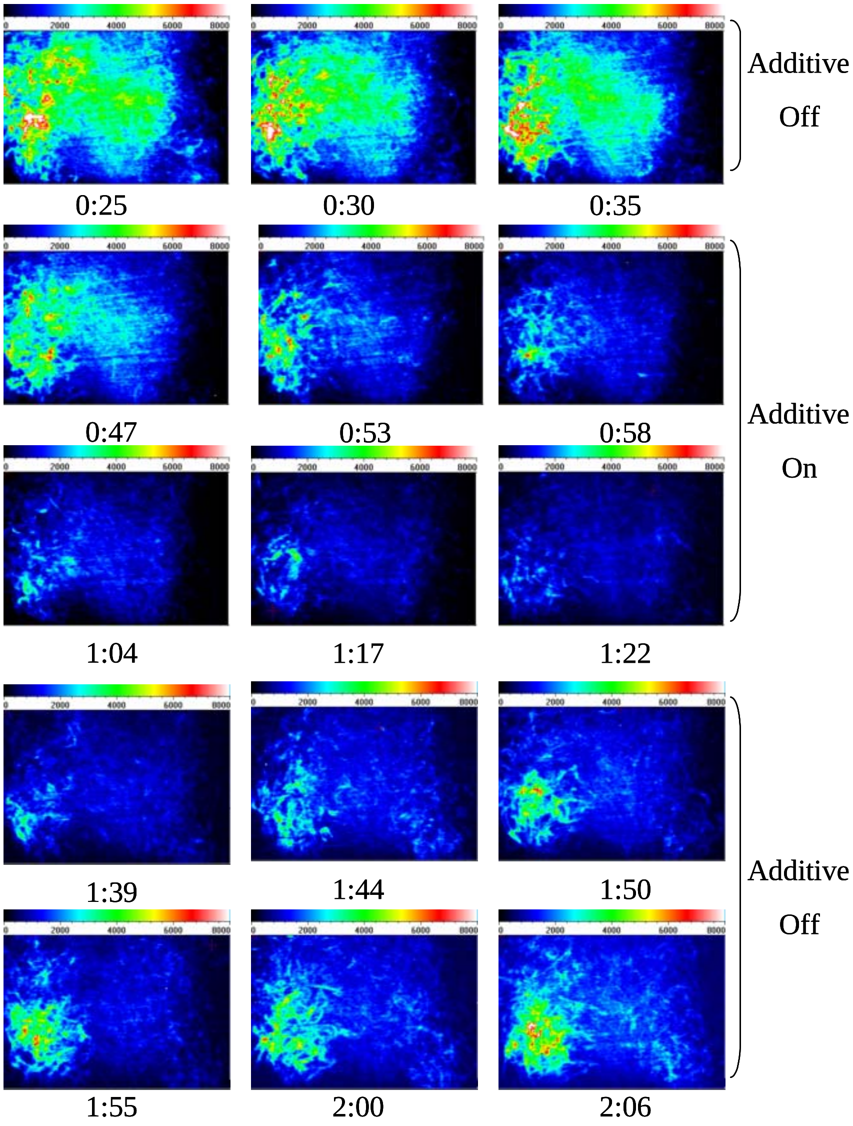

Figure 3.17: Series of LII images illustrating the time dependent behavior of the commercial additive

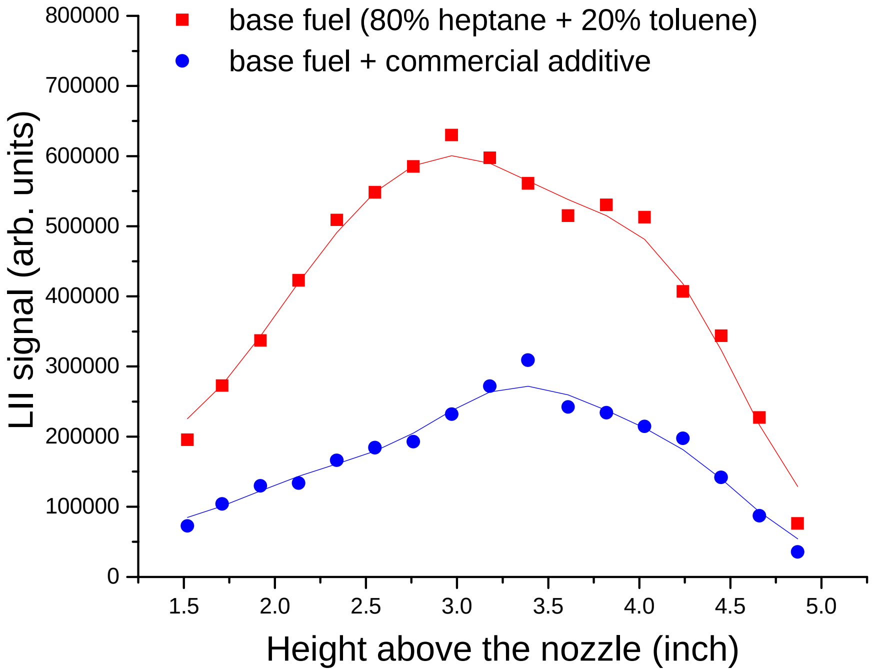

Figure 3.18. Effects of commercial additive on soot

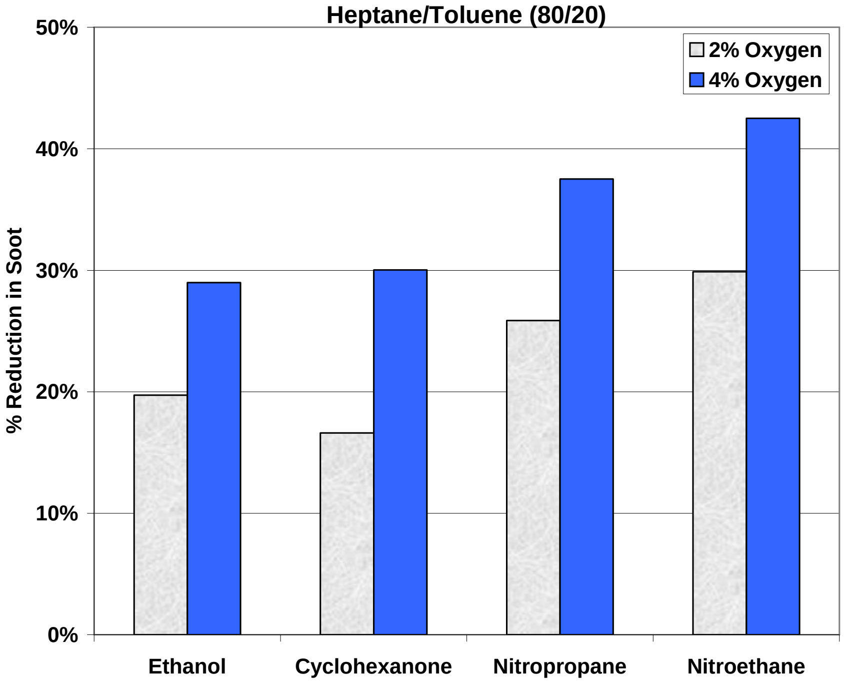

Figure 3.19. Effect of individual components of the commercial additive on soot (ethanol included for comparison purposes.)

3.2.2 HIGH PRESSURE TURBULENT REACTOR

All tests with nitro-alkane additives in the high pressure turbulent combustor were run with JP8 as the fuel; a major consideration being its reasonable cost compared to the heptane/toluene blend. The air flow for the tests was 32 gm/s and the equivalence ratio was 1.3. The inlet air temperature was 550K and the chamber pressure was 0.5 MPa. Only two of the three nitro-alkanes from the commercial additive were studied, nitroethane and nitropropane. The third, nitromethane, can detonate due to compression so it was not run in these experiments.

Figure 3.20 presents a summary of the test results on soot volume fraction versus additive concentration. Nitroethane was added to JP-8 in concentrations ranging from approximately 2.5% to 10% by volume of the fuel. It was found that the nitroethane reduced soot at all concentrations. The soot suppression effect was found to increase with increase in the additive concentrations. At the lowest concentration of about 2.5%, the soot reduction was roughly 20% and at an additive concentration of 10% by volume in the fuel the reduction was ~70%. Similar trends were observed with the addition of nitropropane. Although the reduction in soot was approximately the same as with nitropropane at the lowest additive concentrations, the reduction was slightly lower than nitroethane at higher additive concentrations. At an additive concentration of about 10% by volume of JP-8, nitropropane reduced soot by approximately 60%.

These levels of reduction were substantially greater than those obtained with ethanol. Modeling of the experiments could not be performed with standard tools in CHEMKIN due to the complexity of the flow-field so the reasons for the greater effectiveness observed could not be identified through modeling.

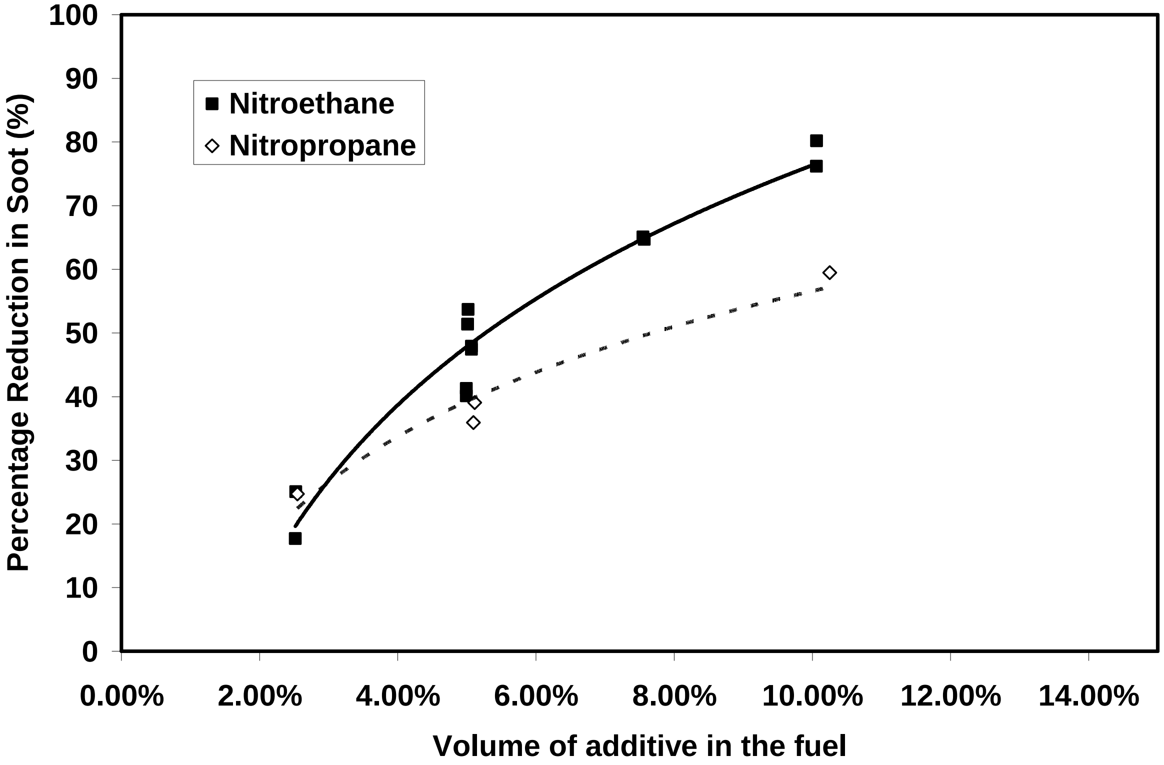

Figure 3.20: Effect of nitroalkanes on soot formation in the dump combustor with JP-8

3.3 NITROGEN DIOXIDE

Due to the fact that NO_2 was identified as a major intermediate in the reduction of soot by the nitroalkane species, experiments were run with NO_2 addition to understand its direct effect on soot. Experiments with NO_2 addition were performed in the shock tube at UDRI and in a premixed flame at Penn State. Since the Penn State premixed flame facility was not set up to utilized prevaporized liquid fuels, experiments were performed with ethylene as the fuel.

3.3.1 PREMIXED FLAME

A premixed flame of ethylene (99.9%) and air at 1 atm was stabilized on a 60mm stainless steel water-cooled porous plate, surrounded by a 6mm wide porous annulus to provide a shroud of nitrogen (99.5%) to help shield the flame from the surroundings. The flame was stabilized using a 125mm diameter circular aluminum plate with a 30mm hole in the center that was mounted 32mm above the burner surface. This setup, which yielded a very stable flame, matched those used by Xu *et al.* (1997). The entire assembly was mounted on a two-dimensional linear translation stage controlled by stepper motors (±0.0254mm). All reactant flows were controlled using mass flow meters (±0.1% at full scale) and all secondary flows such as cooling water and co-flow nitrogen were controlled using calibrated rotameters. A mixture of NO_2 at a concentration of ~10,000 ppm in air was then added to additional air and ethylene streams that were passed into a mixer which consisted of a 10mm inner diameter, 1m long stainless steel pipe with stainless steel washers placed every 20mm to enhance mixing.

The flow conditions for these laminar premixed ethylene-air and ethylene-air-NO2 flames for the two equivalence ratios studied are tabulated in Table 3-10. The C/O ratio and mass flux across the burner were maintained constant for both the baseline and the flames with NO2 added. The adiabatic flame temperature as calculated from the CEA chemical equilibrium code (Gordon and McBride, 1996) was maintained constant for the baseline flame and the flames with NO_2 added, by adding a small quantity of nitrogen to the flow.

Figure 3.21 shows the profiles of soot volume fraction, temperature and normalized CH* emission for the baseline (BL) flames and flames with NO_2 added at the equivalence ratios of 2.34 and 2.64 as a function of the height above the burner (HAB) surface. For both equivalence ratios, a reduction in the soot volume fraction, fv, is observed when NO_2 is added. For the Φ=2.34 flame, a reduction of about 15% is observed at the final measurement point of 22.5mm HAB. For Φ=2.64, the fv profiles exhibit a similar trend as seen in the Φ=2.34 flame, however, the reduction in soot with the addition of NO2 is seen to be significantly greater. In the baseline flame at Φ=2.64 the maximum fv is observed to be around 1.1 ppm at 22.5mm HAB, while the peak value observed with the addition of NO_2 is about 0.8 ppm, a decrease of roughly 30%. It is interesting to note that an increased reduction in fv is seen in the Φ=2.64 flame as compared to the Φ=2.34 flame when NO_2 is added.

The temperature measurements are shown in Fig. 3.21b. All measured baseline temperatures fall below the adiabatic flame temperature of 1728K for Φ=2.34 and 1578K for Φ=2.64 calculated from the chemical equilibrium code (Gordon and McBride, 1996). The temperature increases sharply until about 6mm HAB where it plateaus until approximately 12mm HAB, after which a gradual decrease in the temperature is observed. For both equivalence ratios, the peak temperatures and its axial location are nearly identical for both the baseline flame and the flame where NO_2 is added. For both equivalence ratios, the measured temperatures for the flame where NO_2 is added are slightly lower (10 to 25 K) than for the baseline flame below 12mm HAB. However, higher up in the regions that contain soot particles, temperatures of the flames with NO_2 added are slightly higher than for baseline flames ($\pm$25K). These measurements confirm that the temperature profiles change very little in location or peak temperatures as intended in the selection of the flow conditions. These temperature profiles are used as the input data for the modeling analysis.

The axial location of the reaction zone was also determined from the CH* chemiluminescence emission at 431nm using the same optical setup as used in the line reversal method. As shown in Fig. 3.21c, the location of the peak in the CH* profile remains unchanged with the addition of NO_2 for both equivalence ratios. The axial location of the CH* peak also corresponds to the region of maximum gradient in the temperature profiles shown in Fig. 3.21b, another indicator of the location of the reaction zone.

Figure 3.22 shows the measurements of Qvv, Qhv and Qf profiles at the two equivalence ratios for the baseline flame and the flame where NO_2 is added. This figure yields a broad overview of the evolution of the soot particle field starting with the fuel molecules. Examination of Qvv profiles for the baseline flame at Φ=2.64 shows that the light scattering measurement, Qvv, is significantly greater than the Qhv and Qf measurements very near the burner surface until a height of approximately 3mm HAB. This result is due to the relatively strong Rayleigh scattering by the gases in the region comprised of the initial byproducts of fuel pyrolysis and oxidation processes. Between approximately 3mm and 6mm above the burner, Qvv, Qhv and Qf are observed to be comparable in magnitude. A sharp rise in Qvv is observed at a height of approximately 6mm HAB, possibly corresponding to the point of inception of soot particles, given the magnitude of the observed increase. It should be noted that in this region and up to a height of approximately 7.5mm, Qhv and Qf are approximately equal in magnitude, indicating that both signals have a common source i.e., both are due to fluorescence which is depolarized. Above 7.5mm HAB, a clear separation of Qhv from Qf is observed, indicating a departure from the Rayleigh theory of light scattering from small particles since Qhv = 0 at a 90° angle in the Rayleigh limit. The source of such a departure from Rayleigh theory could be due to the occurrence of non-spherical particles resulting from the agglomeration of incipient soot particles formed lower in the flame.

In the flames to which NO_2 is added, light scattering near the burner surface is equal to that observed in the baseline case up to a height of approximately 2mm HAB. However, Qvv remains higher than both Qf and Qhv in the flames that contain NO_2 until 4mm HAB when compared to the baseline case. This result indicates that the formation of the species which contribute to the fluorescence in this region has been delayed by approximately 2mm. The same shift is seen in the location where Qvv increases above the depolarization, Qhv, and fluorescence, Qf, profiles, and for the location where Qhv rises above the Qf.

Figure 3.22c shows specifically the fluorescence signals shown in Figs. 3.22a and 3.22b to provide additional clarity. Broadband fluorescence identical to that observed in these flames is widely considered to be an indicator of the presence of PAH species in hydrocarbon flames. Although fluorescence originates from a wide range of aromatic species, these are two very similar flames as indicated by the measured temperature profiles. Thus, the relative difference in the intensities of the fluorescence signal of the baseline flame and the flame with NO_2 added is argued to be due to a change in the concentrations of the aromatic species under these particular conditions. For the Φ=2.34 flame, it is seen that the fluorescence signal with the addition of NO_2 is lower than the baseline case earlier in the flame until about 5mm HAB, but for HAB greater than 5mm, the fluorescence signal in the flame with NO_2 added is higher than in the baseline flame. This crossover point is also seen in the Φ=2.64 case at an HAB of approximately 9mm. The wavelength of the fluorescence signal from PAH is dependent on the number of aromatic rings present in the excited species. The fluorescence signal at 514.5nm used in the present study is indicative of the presence of aromatic species of four rings or greater (Kohse-Höinghaus and Jeffries, 2002).

To gain further insight into these observations, the chemical kinetic modeling results must be discussed. There are two key factors to be noted about the modeling results that are presented and its analysis: 1) The reactions in this mechanism and the corresponding rate constants are pertinent to the interpretations of the chemical pathways and possible explanations of the observed experimental results. 2) The model captures the kinetics of the flame only through the formation of PAH species and does not consider soot formation or growth. However, since PAH are widely regarded as the precursors of soot, a study of the formation of PAH will give insight into the soot inception process. The modeling results for $\Phi=2.64$ are discussed.

With the aid of Xsenkplot, the integrated carbon flux from C_2H_4 to C_6H_6 was analyzed using the rates of production of the intermediate species such as C_2H_3 (vinyl), C_2H_2 (acetylene) and H_2CCCH (propargyl). This analysis follows the method outlined by Song *et al.* (2003). Competing oxidation and other 'non-soot' reactions were also considered for each species. This carbon flux diagram is shown in Fig. 3.23; the numbers indicate the percentage flow of carbon to each species relative to the fuel concentration with the NO_2 case shown on the right. The soot path is shown with bold arrows and bold lettering. The oxidation pathways are considered relative to the parent species and not to the fuel. Considering the formation of the vinyl radical, it is seen that 72.8% of C_2H_4 is converted to C_2H_3 in the flame where NO_2 is added in comparison to the 73.0% conversion in the baseline flame. Following the path to soot, in the baseline case, 41.3% of the fuel is converted into acetylene, while 39.4% of the fuel is converted to acetylene with the addition of NO2. Similarly for the propargyl radical, the fuel conversions are 3.8% and 3.3% for the baseline flame and the flame with NO_2 added, respectively. At the final step in the path to soot precursors, 2.0% of the C_2H_4 goes to forming benzene in the baseline case, whereas in the flame with NO_2 added the conversion drops slightly to 1.9%. Thus in the flame with NO_2 added, key intermediates in the reaction pathway from the fuel to benzene and benzene itself are reduced relative to the baseline flame in the pre-soot inception region. Interestingly however, the acetylene concentration shifts to being higher for the flame with NO_2 added, at approximately 2.5mm HAB (see Fig. 3.25).

Analysis of the modeling results was undertaken to explain these trends. The first species that were investigated were key chain-carrying radicals, H, OH, and O. The H atom concentrations shown in Fig. 3.24 are lower for the flame with NO_2 added until 2.5mm HAB. The initially lower levels of H atoms appear to be due to the reaction $NO_2+H \rightarrow NO+OH$ in the flame where NO_2 was added and the lower temperatures of this flame (approximately 25 K lower near the burner) that lead to lower rates of production of H atoms via decomposition of C_2H_3. At lower HAB, the hydroperoxy (HO_2) radical concentrations are also considerably lower with the addition of NO_2; the major route of depletion being the reaction $NO+HO_2 \rightarrow NO_2+OH$ (Mueller, *et al.*, 1999). The decrease in H and HO_2 concentrations in the flame with NO_2 added is reflected in a similar decrease in the OH concentrations, by way of the reactions HO_2+H→2OH and H+O_2→OH+O. The lower reaction rate of C_2H_3 decomposition also leads to lower formation rate of acetylene at low HAB. However, near 2.5 mm the concentrations of H and OH radicals for the flame where NO_2 is present become higher, leading to increased formation of vinyl radicals that subsequently form acetylene.

The lower acetylene concentration at lower HAB leads to lower propargyl concentrations and subsequently lower benzene concentrations as shown in Fig. 3.25. On the other hand, the higher concentration of C_2H_2 downstream of the soot inception zone is instrumental in yielding the higher concentrations of the large PAH in that region. For instance pyrene ($C_{16}H_{10}$), a four ringed aromatic compound is formed predominantly by a C_2H_2 addition reaction involving the phenanthrene radical ($C_{14}H_9$), $C_{14}H_9+C_2H_2 \rightarrow C_{16}H_{10}$ +H. The increase in C_2H_2 higher in the flame corresponds to an increase in the concentrations of pyrene as seen in Fig. T-5. Similarly the formation of coronene ($C_{24}H_{12}$) involves the addition of acetylene to Benzo[ghi]perylene ($C_{22}H_{12}$) by the reaction $C_{22}H_{12}$ +$C_2H_2 \rightarrow C_{24}H_{12}$. A lower concentration of coronene near the burner surface and a subsequent increase higher up in the flame correlates with the trend seen in the C_2H_2 profile.

The major route for the formation of phenanthrene (A3, $C_{14}H_{10}$) is through the reaction of the indenyl radical (C_9H_7) with cyclopentadienyl (C_5H_5) radical; $C_9H_7+C_5H_5 \rightarrow C_{14}H_{10}+H_2$. The indenyl radical is formed from indene (C_9H_8) primarily by the reaction $C_9H_8+H \rightarrow C_9H_7+H_2$. However, indene is formed from acetylene and the benzyl radical (C_7H_7) by the reaction $C_7H_7+C_2H_2 \rightarrow C_9H_8+H$. The major reaction for the formation of C_5H_5 is the dehydrogenation of cyclopentadiene via $C_5H_6+H \rightarrow C_5H_5+H_2$. The lower acetylene concentrations in the pre-soot inception region slow down the formation of indene and in turn, the formation of the indenyl radical. In addition, the lower H atom concentrations slow the formation of the cyclopentadienyl radical. These result in a lower concentration of phenanthrene in the pre-soot inception region. Moreover, as can be seen from Figs. 3.24 and 3.25, when the C2H2 concentrations in the flame with NO2 added become higher than in the baseline case, a corresponding rise is seen in the A3 (phenanthrene) profiles for the flame with NO2 added. Thus, when provided with the experimentally measured temperature profiles, the model produces trends in aromatic species that are consistent with the cross-over that is observed in the fluorescence signals (see Fig. 3.22c and Fig. 3.25(top)). The modeling also predicts lower levels of soot precursor species in the region prior to soot inception that are consistent with the observations of lower soot levels in the flame with NO_2 added.

Table 3-10: Experimental Conditions

Φ		2.34		2.64	
Condition		Base flame	5% NO_2	Base Flame	5% NO_2
C/O Ratio		0.78	0.78	0.88	0.88
Air Flow rate	(mg/s)	194.3	39.0	190.9	19.1
Air/NO_2 Flow rate	(mg/s)	0.0	149.7	0.0	166.1
Nitrogen Flow rate	(mg/s)	0.0	5.8	0.0	5.8
Fuel Flow rate	(mg/s)	30.8	30.7	34.1	34.0
Co-flow Nitrogen Flow rate	(mg/s)	557.0	557.0	557.0	557.0
		Mole fractions			
C_2H_4		0.1408	0.1410	0.1560	0.1567
O_2		0.1805	0.1734	0.1773	0.1698
N_2		0.6787	0.6782	0.6667	0.6652
NO_2		-	0.0074	-	0.0083

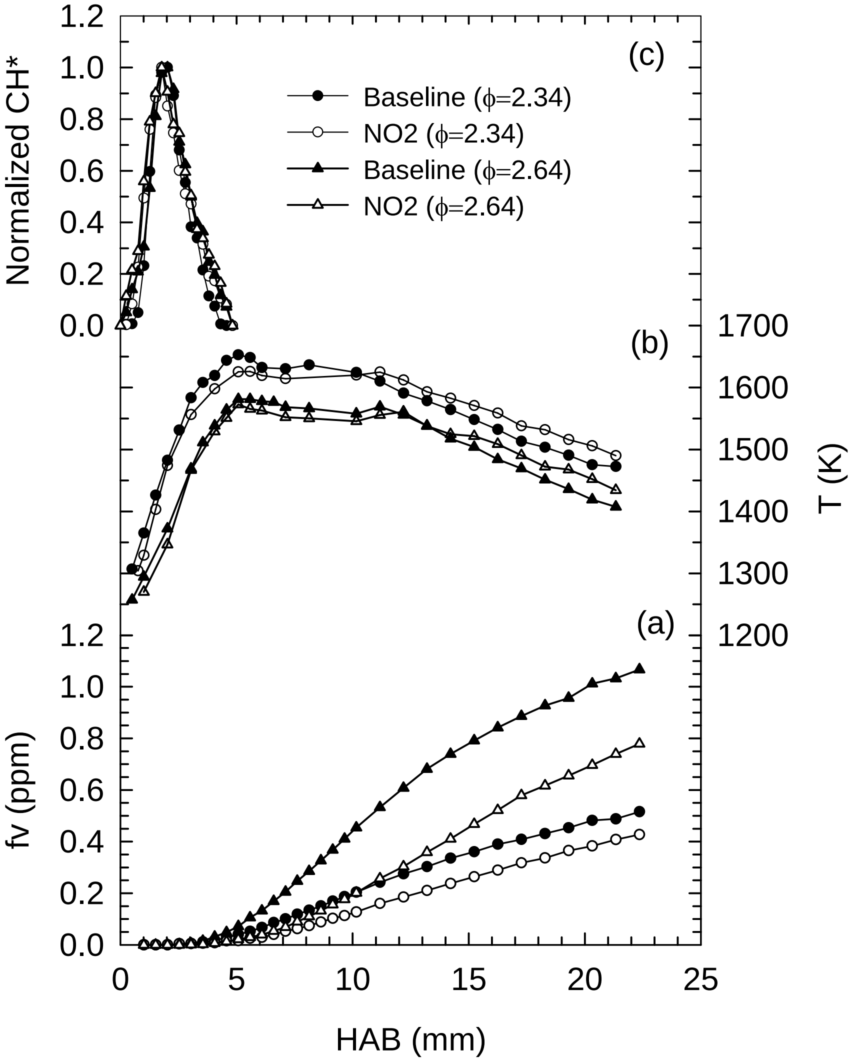

Figure 3.21: The axial profiles of (a) fv, (b) temperature and (c) normalized CH* emissions for two equivalence ratio of 2.34 and 2.64. Solid symbol: baseline and open symbol: NO_2-addition.

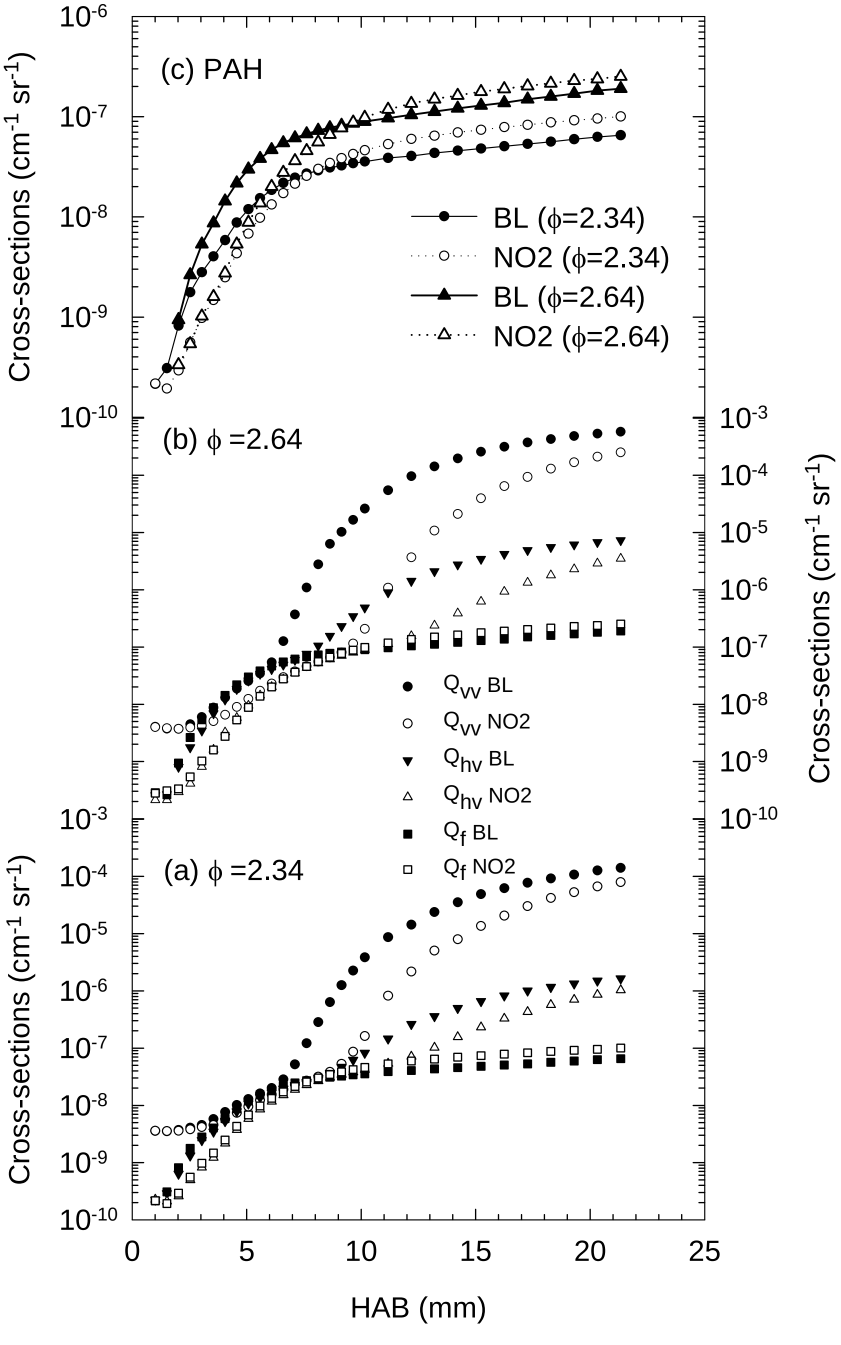

Figure 3.22. Polarized (Q_{vv}), depolarized (Q_{hv}) scattering and fluorescence (Q_f) signals for (a) Φ=2.34, (b) Φ=2.64 and (c) PAH vs. HAB. Solid symbol: baseline and open symbol: NO_2-addition.

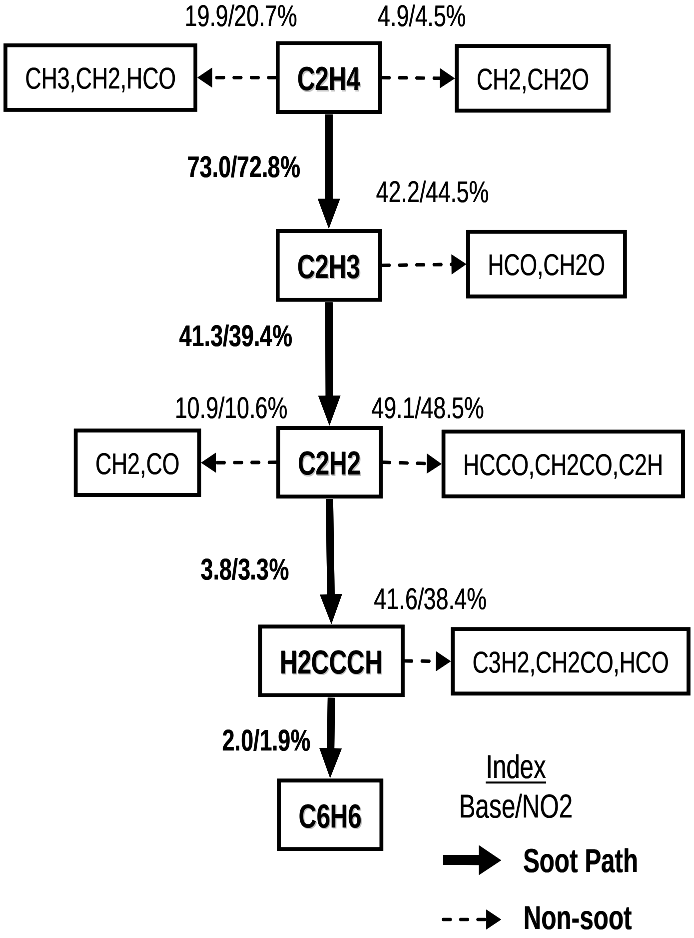

Figure 3.23: Absolute carbon flux map comparing baseline and NO_2 addition for Φ=2.64

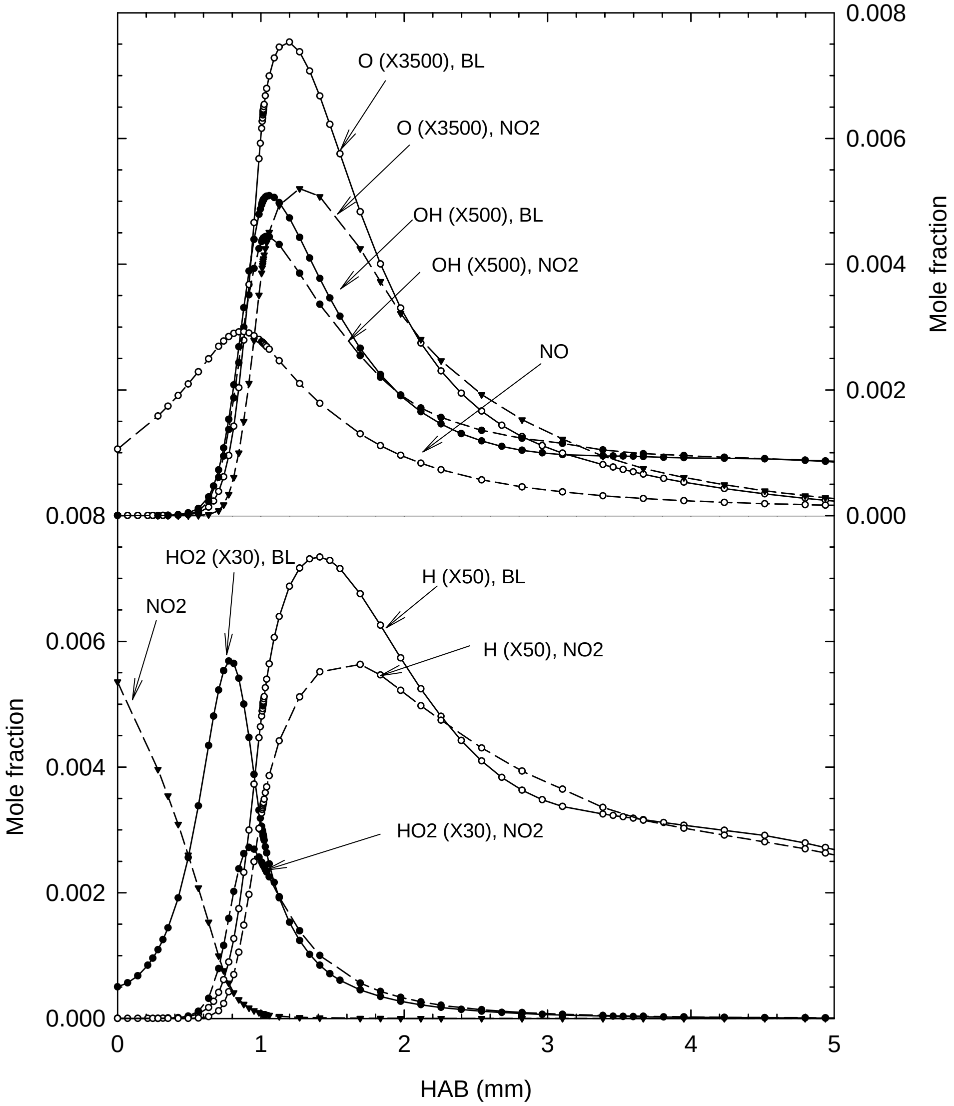

Figure 3.24. Minor species at Φ=2.64. Solid line: baseline and open line: NO_2-addition.

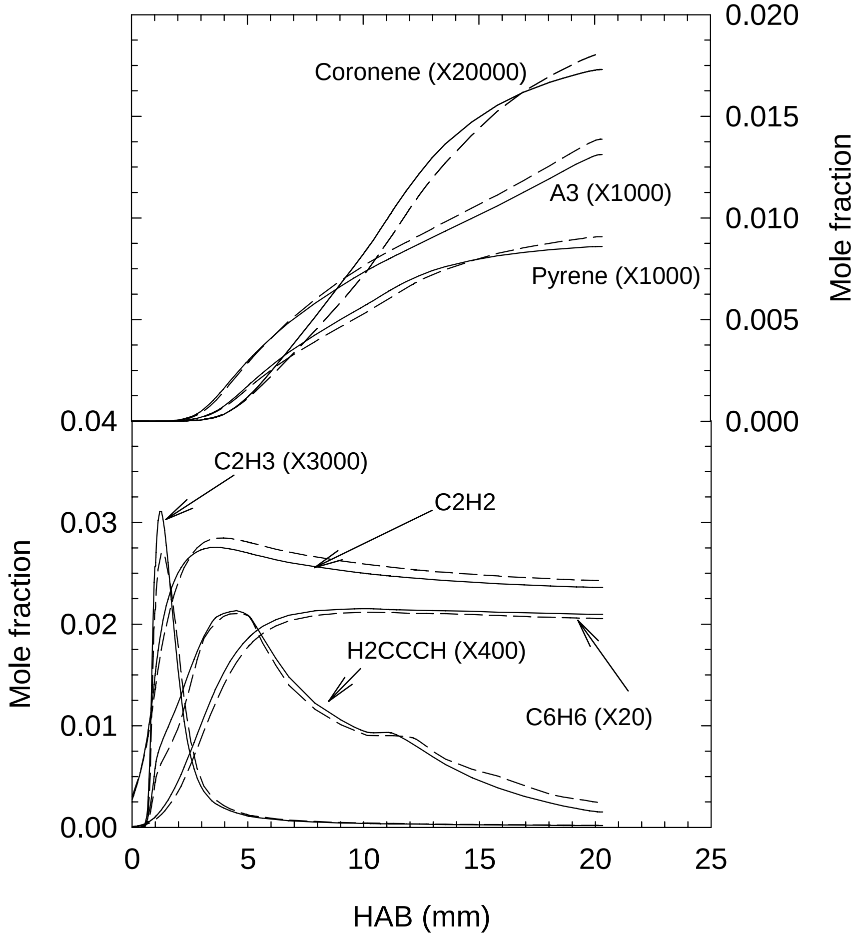

Figure. 3.25. Carbon species (bottom) and aromatic species (top).

3.4 PYRIDINE

The study of nitroalkanes triggered a thought process that led the team to consider other species containing heteroatoms that might reduce soot, which eventually led to testing of pyridine. Pyridine, a six membered ring containing 5 carbons and one nitrogen, is known to pyrolyze without forming soot. Initial studies in a premixed flame showed substantial reductions in soot and led to the study in the full suite of devices.

3.4.1 TURBULENT SPRAY FLAME

In spite of the difficulties in getting repeatable results in the spray flame, it was still useful in obtaining results on the effects of additives. After discovery of the problem with repeatability experimental procedures were modified to allow for real-time addition of the additive so that day-to-day repeatability was not an issue. It was in this mode that the burner was used to investigate the effectiveness of pyridine on soot. The experimental conditions were similar to those used for the commercial additive tests. Precisely equivalent conditions could not be established due to problems with nozzle fouling and subsequent cleaning which modified flow characteristics. Pyridine was added at 10% by volume to ensure that any effect from the additive would be clear in the measurements.

Figure 3.26 presents the time dependent plot of the LII signal with and without the pyridine additive for the heptane/toluene fuel. The results show a substantial reduction, on the order of 40%, for this level of pyridine addition.

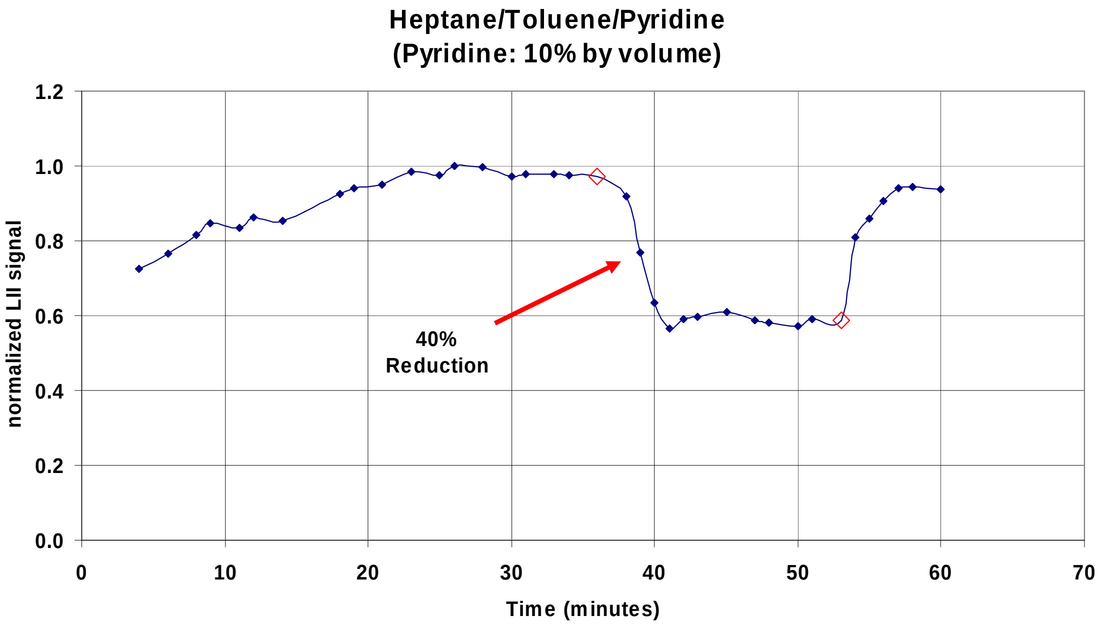

Figure 3.26. Effect of pyridine on soot in the turbulent spray flame

3.4.2 <u>HIGH PRESSURE TURBULENT REACTOR</u>

Initial tests with pyridine were run with JP8 as the fuel. The air flow for the tests was 32gm/s and the equivalence ratio was 1.3. The inlet air temperature was 550K and the chamber pressure was 0.5MPa. The results showed little effect of pyridine in contrast to the results from the turbulent spray burner and premixed flame results. At the annual IPR in 2005, a suggestion was made that experiments be performed with heptane/toluene to investigate the effect of fuel composition on the results. Consequently, runs with pyridine in heptane/toluene were performed under similar experimental conditions to the JP8 experiments.

Figure 3.27 presents a summary of the test results on soot volume fraction versus additive concentration for JP8 and heptane/toluene. Pyridine was added at 5 and 10% by volume. The measured soot volume fractions with and without pyridine in the fuel stream indicate that there was a small reduction in soot by the additive. For JP8, the decrease in soot concentrations was approximately 3% at an additive concentration of 5% by volume and approximately 10% at an additive concentration of 10% by volume. Both of which are within the measurement uncertainty for the extinction method used. The experiments with heptane/toluene showed even smaller reductions in soot levels when pyridine is added. The results lead to two conclusions.

First that pyridine is not effective in reducing soot under conditions which simulate actual combustor conditions, and secondy that the fuel composition does not account for the lack of an effect on soot.

It appears then that the pyridine is not effective at the higher pressure conditions in this reactor compared to the atmospheric pressure spray flame. The reason for this effect could not be determined from modeling because the chemical mechanism for the pyridine/heptane/toluene mixture proved to be inadequate, even for the shock tube experiments.

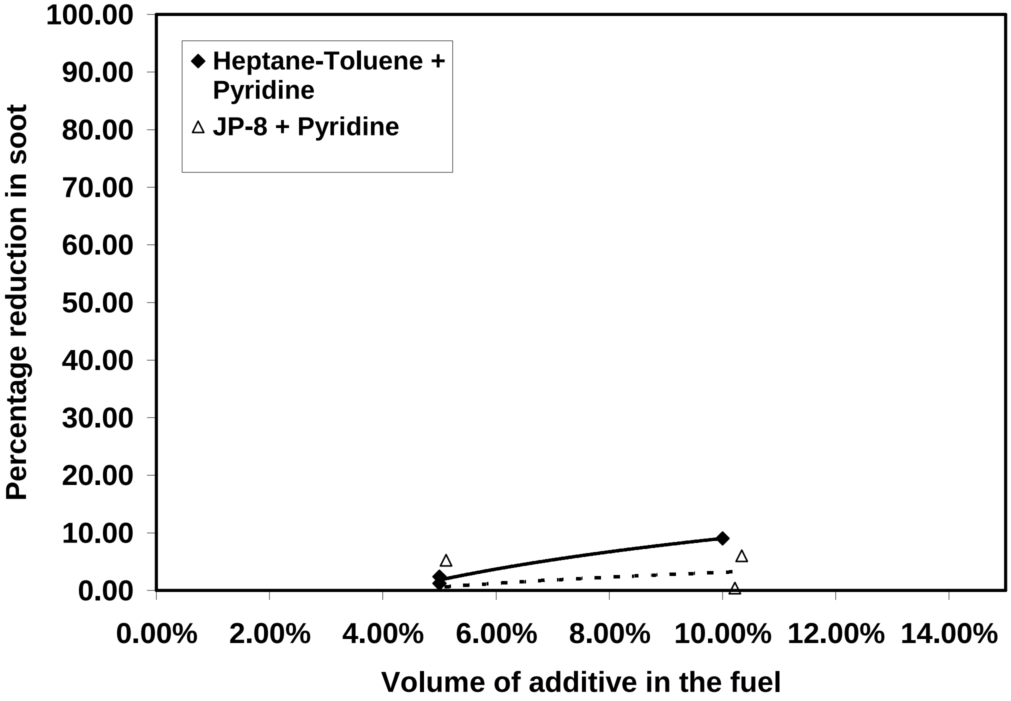

Figure 3.27: Effect of pyridine on soot formation in the dump combustor with JP-8

3.5 PHOSPHORUS

The work performed was essentially screening studies to determine if the phosphorus showed sufficient reductions in soot to merit more detailed testing. Experiments were performed in the a premixed flame and a co-flow diffusion flame because this type of flame was used in the prior study at NBS that motivated the investigation.

3.5.1 PREMIXED FLAME

The experiments were conducted on a laminar premixed flat flame burner using ethylene (C_2H_4) as the fuel and air as the oxidizer. The flame was shielded from the surrounding air using a shroud of nitrogen supplied through an annulus 11mm thick, concentric to the burner, which was 60.3 mm in diameter. The soot volume fraction was measured using laser extinction, using the 514.5 nm line of an Argon-Ion laser (Coherent Innova 70).

The total mass flow rate of the fuel-air mixture was approximately 225mg/s. The additive was introduced into the reactant stream by passing the reactants flow through a bed a glass beads ~4mm in diameter and filled with the trimethyl phosphate (TMP). Using the vapor pressure of TMP, it was estimated that the concentration of TMP in the reactant stream was approximately 0.1% by volume of the reactant stream or 0.7% by mass of the reactant stream. The experiment was conducted for equivalence ratios of 2.34 and 2.64, conditions used in all of the other premixed flame experiments conducted at Penn State. The flow conditions for the experiment are presented in Table 3-11.

Experiments were also attempted with propane in order to allow direct comparison to the work of Hastie and Bonnell. However, the flame was just beginning to produce soot at the higher equivalence ratio of 2.64 and at those conditions it was beginning to become unstable. Consequently, no data could be collected for propane with and without TMP added. The difference between the present experiments and those of Hastie and Bonnell is the type of burner used. They used a small diameter premixed jet flame that could be stabilized at much richer conditions that the flat flame used in this study. The flat flame burner is necessary to allow optical diagnostics to be used.

The soot volume fractions for the baseline and the flame with TMP added for an equivalence ratio of 2.34 is shown in Figure 3.28. It is seen that the soot volume fractions for the flame with TMP added are slightly higher than the baseline flame, the increase in soot at the last measurement point being approximately 3%, which is within the uncertainty of error for the technique. The same trend is seen in Figure 3.29 at an equivalence ratio of 2.64; but the increase in soot in slightly higher than the leaner flame, with an increase of approximately 6.5% at the final measurement point of 20 mm HAB.

Within this program, an increase of soot was observed when ethanol was added to ethylene-air opposed-flow diffusion flames due to similar effects. Analysis of modeling results showed that the increase was due to the methyl radicals formed from the ethanol which increased the rate of formation of the first aromatic ring via a 4-carbon intermediate. The increase of soot with the addition of TMP may be a result of a similar effect.

Table3-11: Flow Conditions for Premixed Ethylene Flames with TMP

Flame	**Baseline**	**Additive**	**Baseline**	**Additive**
Equivalence Ratio	2.34	2.34	2.64	2.64
C/O ratio	0.78	0.78	0.88	0.88
Fuel mass flow rate (C_2H_4), mg/s,(cc/s)[a]	30.8 (26.45)	30.8 (26.45)	34.1 (29.28)	34.1 (29.28)
Air mass flow rate mg/s,(cc/s)[a]	194.3 (161.93)	194.3 (161.93)	190.9 (159.09)	190.9 (159.09)
TMP mass flow rate mg/s,(cc/s)[b]	0	1.19 (0.20)	0	1.19 (0.20)
Coflow N_2 mass flow rate mg/s,(cc/s)[a]	557 (478.28)	557 (478.28)	557 (478.28)	557 (478.28)
Pressure (atm)	1	1	1	1
Temperature (K)	295	295	295	295
Fuel	Ethylene (99.5%)	Ethylene (99.5%)	Ethylene (99.5%)	Ethylene (99.5%)

a: volumetric flowrate calculated based on T=293K
b: TMP mass flowrate calculated based on T=293K and vapor pressure (110Pa at 293K)

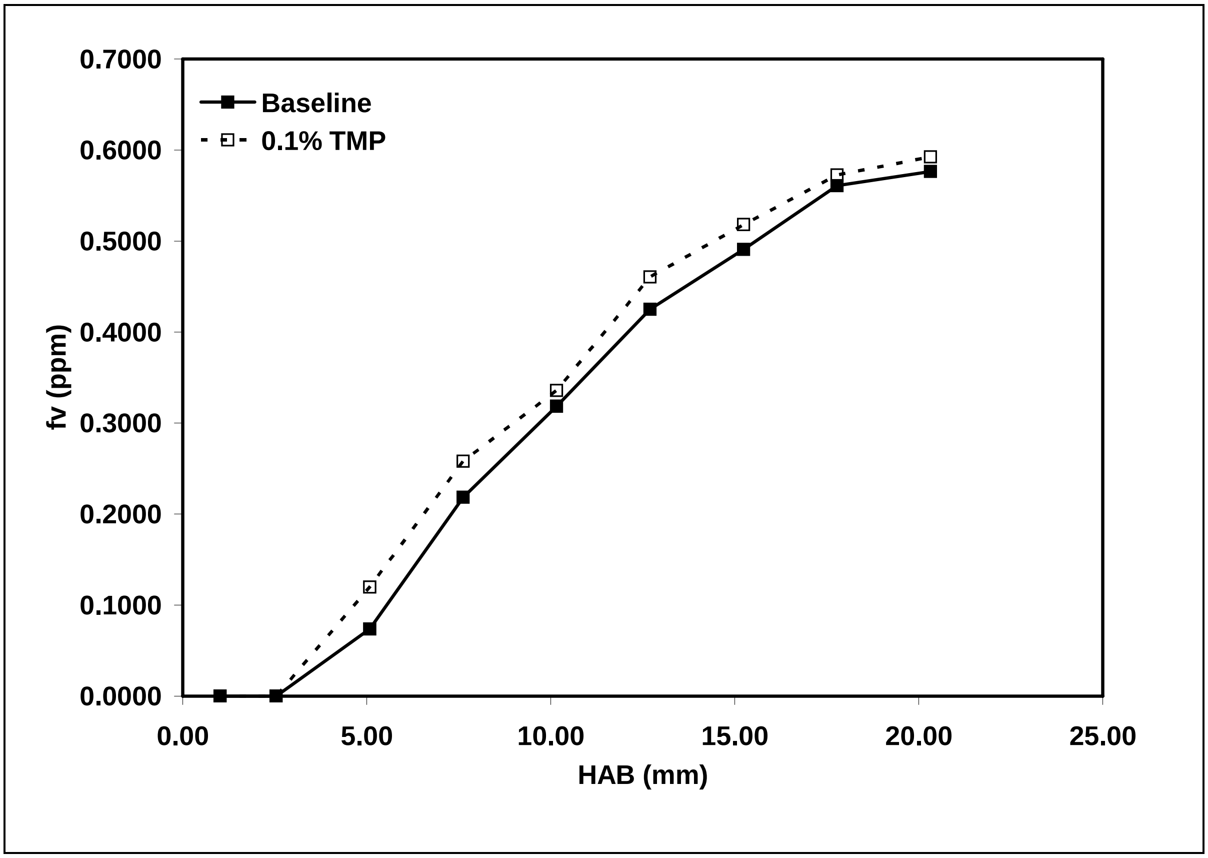

Figure 1.28: Effect of TMP on soot volume fractions for Phi = 2.34 Premixed C_2H_4 Flame

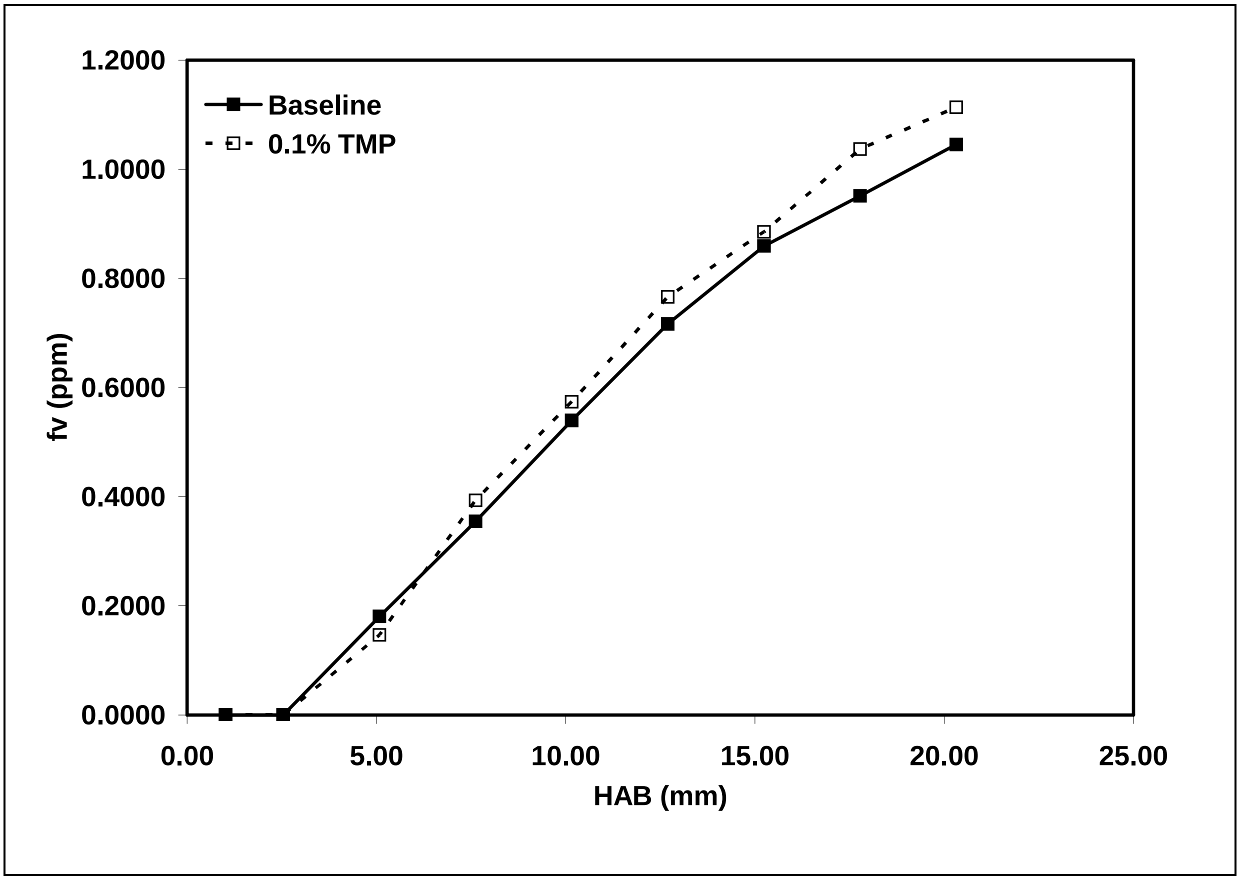

Figure3.29: Effect of TMP on soot volume fractions for Phi = 2.64 Premixed C_2H_4 Flame

3.5.2 CO-FLOW DIFFUSION FLAME

The fuels used in the study were ethylene (purity: 99.5%), propane (purity: 99.9%) and ethane (purity: 99.5%). Coflow air was supplied from a laboratory compressor. The volumetric flowrates of ethylene, propane and ethane were 3.85, 2.5 and 4.13 cc/s, while air flow rate was fixed as 713.3 cc/s for each fuel. The TMP (purity ≥ 99%) supplied by Sigma-Aldrich Corp. known as a chemically active flame inhibitor is liquid at room temperature with low vapor pressure (less than 1 torr at ambient temperature). Due to higher boiling point (~197 °C) of TMP, it is impractical to make a vaporizer system. Instead, glass aspirator was fabricated to convey the TMP vapor by the fuel volumetric flow. The volumetric percentage of TMP was approximately 0.1% of fuel volumetric flow rate based on vapor pressure of TMP. Flame running conditions are shown in Table 3-12.

Figure 3.30 shows ‘false-color’ images of the three flames with and without TMP added. The most obvious effects are visible for ethylene and propane in which the TMP delays the appearance of soot increasing the height above the burner at which soot is first observed. For ethane the soot concentration is so low that no differences are visible.

Decreases in soot concentration do occur when TMP is added to the ethylene and propane flames but they are difficult to see from the images. Therefore, radial soot concentration profiles at various heights in the flames are presented in Figures 3.31, 3.32 and 3.33 to show the differences more clearly. (In these figures the solid symbols represent the baseline flame and the open symbols the flame with TMP.) In general differences are most clear at the lowest flame heights. Finally to give a overall sense of the effects on soot, volume fraction was integrated radially at each height according to the equation

$$F_v(z) = \pi\left(\int_0^R f_v(z,r)rdr + \int_{-R}^0 f_v(z,r)rdr\right)$$

Figure 3.34 presents the overall trends showing that phosphorus leads to a decrease in soot for in the ethylene and propane flames. The reduction in soot with the addition of TMP to the propane flame is consistent with the original work of Hastie and Bonnell with this fuel.

Table 3.12. Experimental conditions for co-flow diffusion flame studies with TMP

	Ethylene		Propane		Ethane	
	Baseline	Additive	Baseline	Additive	Baseline	Additive
Fuel flow rate (cc/s)	3.85	3.85	2.5	2.5	4.13	4.13
Coflow air flow rate (cc/s)[a]	713.3	713.3	713.3	713.3	713.3	713.3
TMP flow rate (cc/s)[b]	0	0.00418	0	0.00271	0	0.00448
Ambient temperature (°C)	21.8	21.8	21.8	21.8	22	22
Flame height (mm)[c]	88	88±1	88	88±1	88	88±1
Fuel purity (%)	99.5		99.9		99.5	
Pressure (atm)	1		1		1	

a: Building shop air

b: Volumetric flow rate calculated based on temperature and vapor pressure at 20 °C

c: Maintained same flame heights for flames to keep same residence time

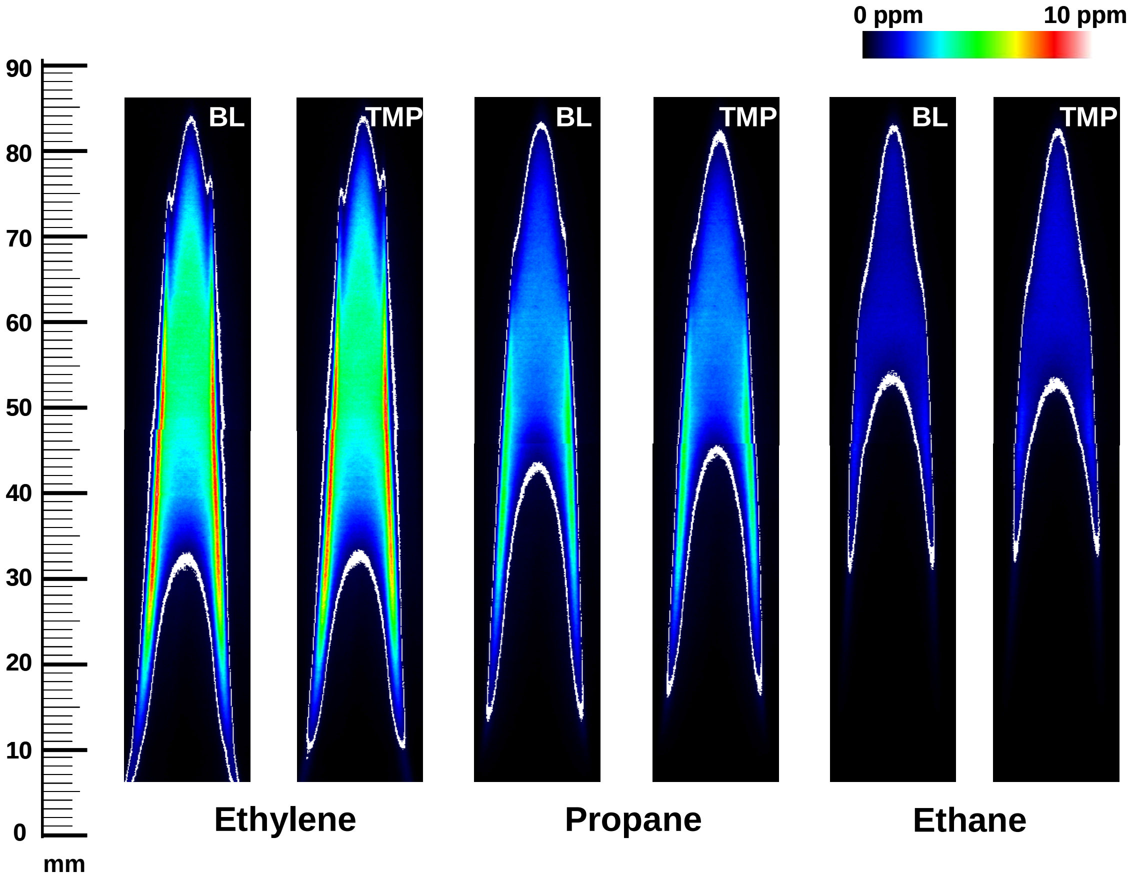

Figure 3.30. Soot volume fraction fields for baseline and TMP addition flames of ethylene, propane and ethane. Contour of fv=0.5 ppm shown in white line is superimposed on soot volume fraction fields.

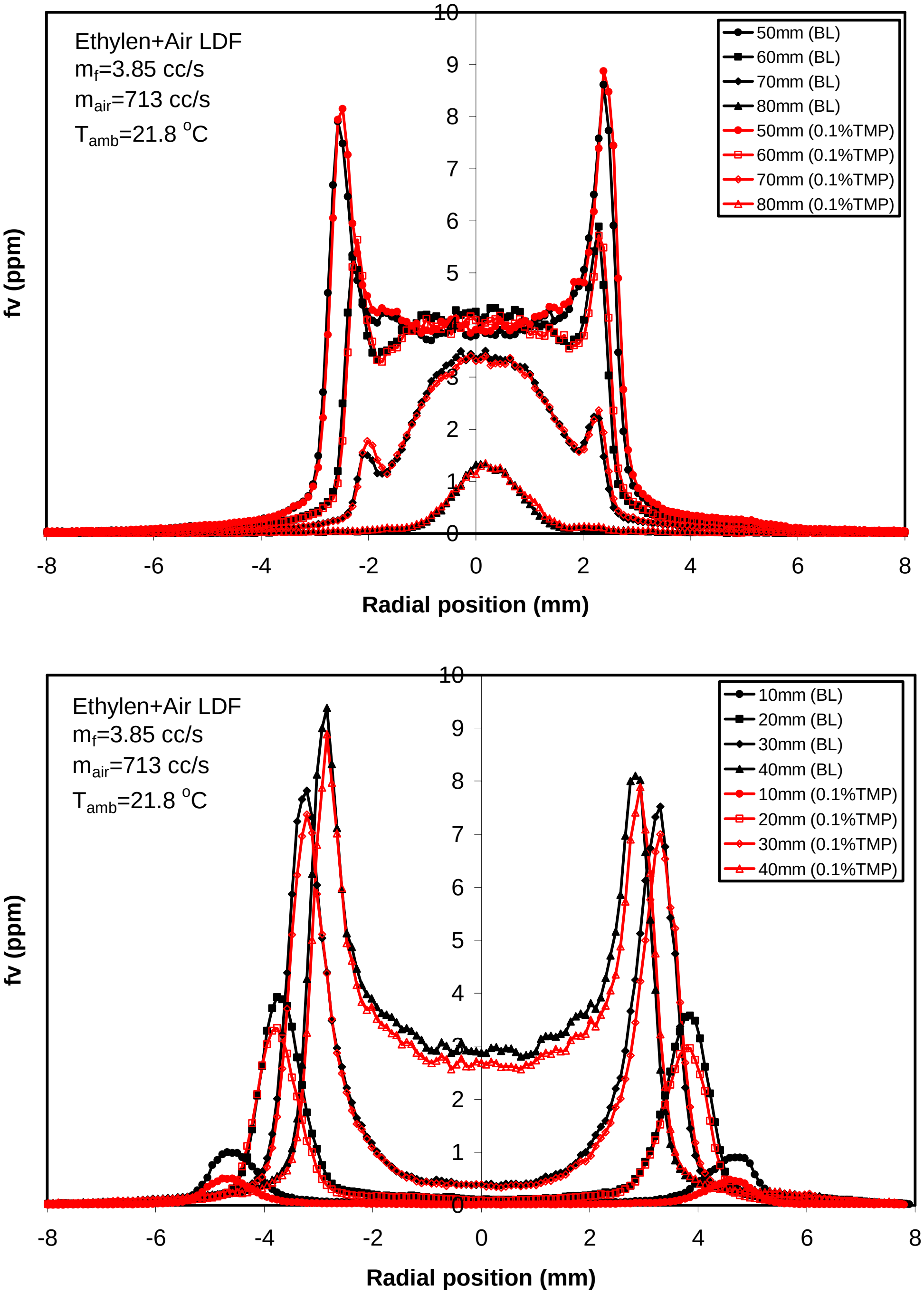

Figure 3.31. Soot volume fraction profiles for ethylene flame with baseline and TMP addition.

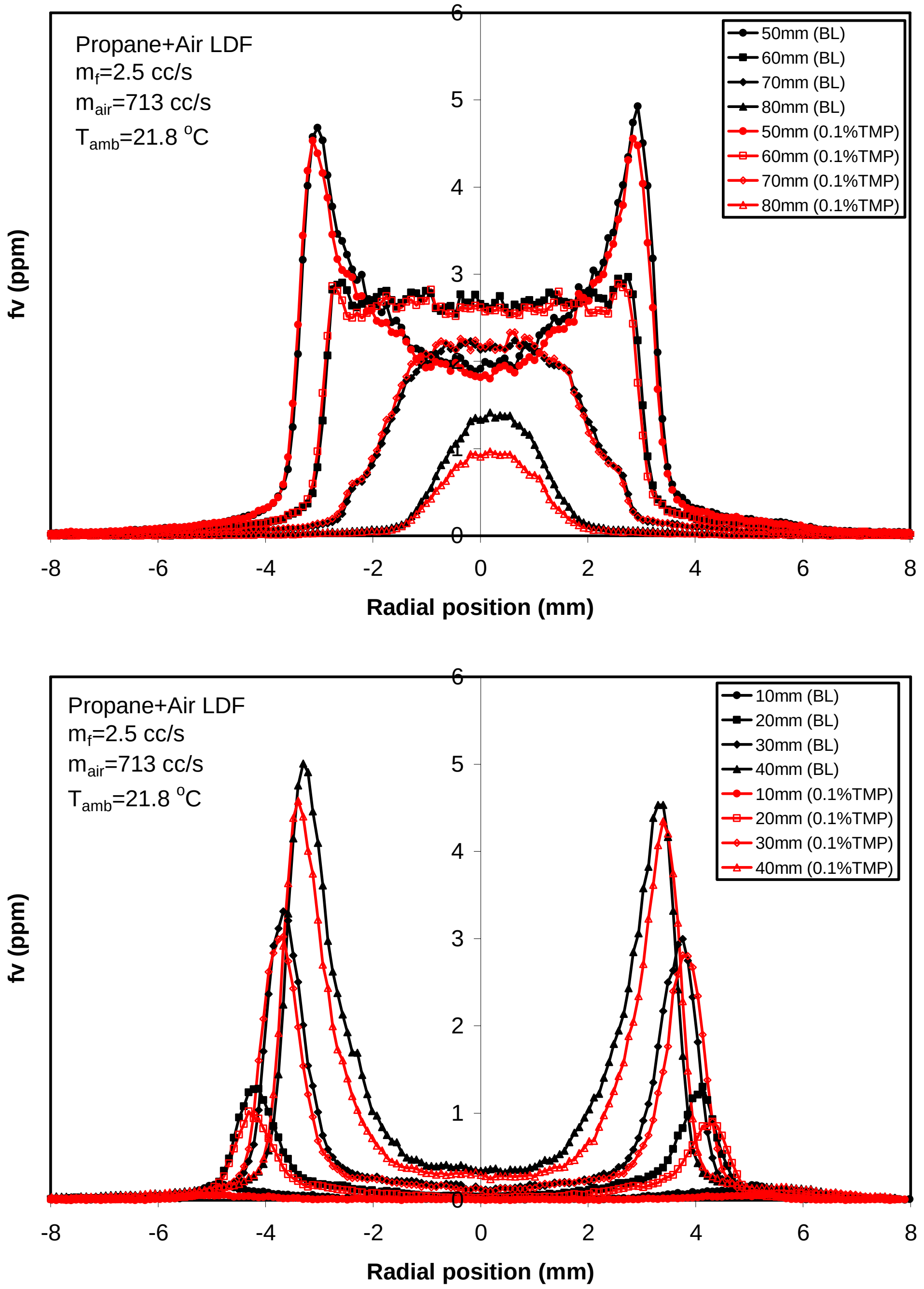

Figure 3.32. Soot volume fraction profiles for propane flame with baseline and TMP addition.

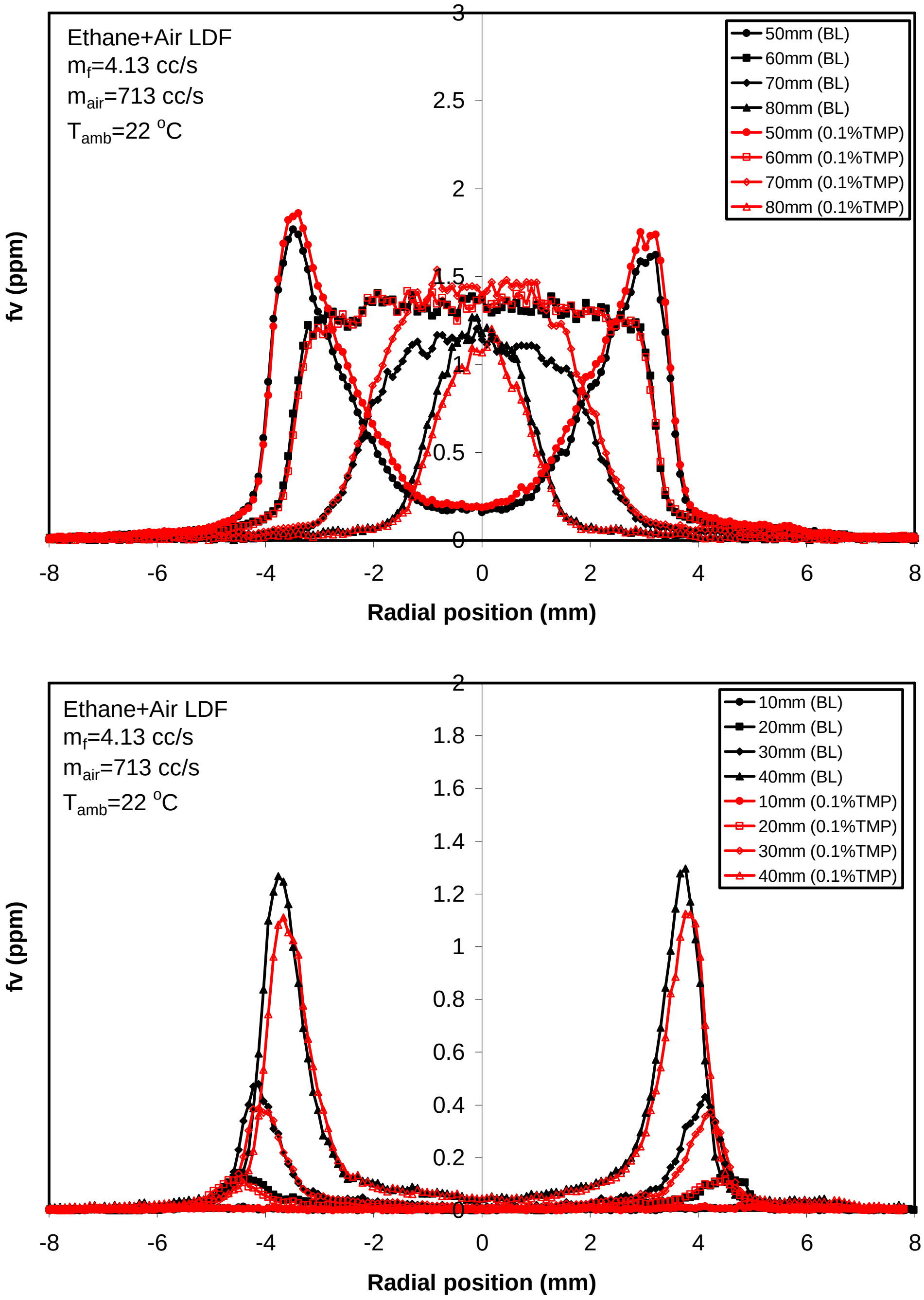

Figure 3.33. Soot volume fraction profiles for ethane flame with baseline and TMP addition.

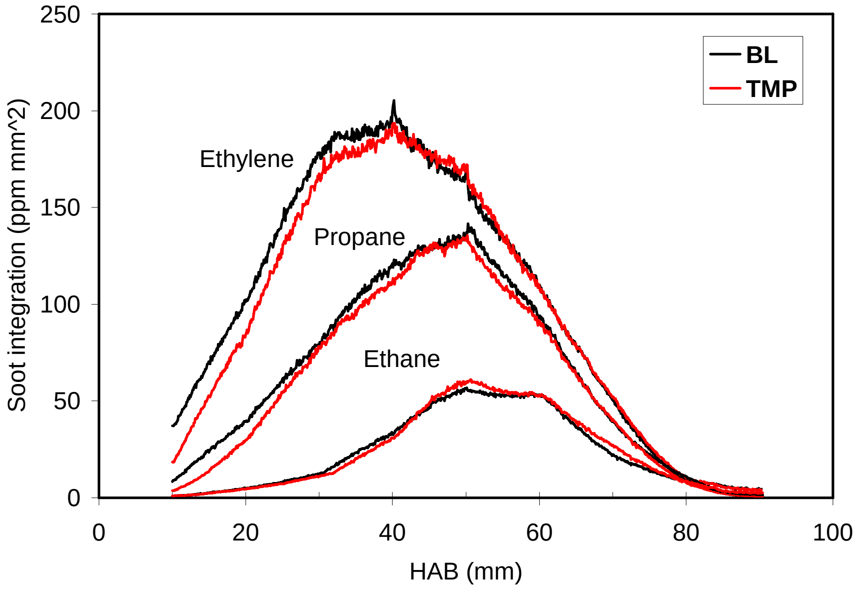

Figure 3.34. Integrated soot volume fraction as a height of the flame.

4. REFERENCES

Beretta, F., A. D'Alessio, A. D'Orsi, P. Minutolo, Comb. Sci. & Tech., 85(1-6), 1992, 455-470.

Curran, H.J. , E.M. Fisher, P.A. Glaude, N.M. Marinov, W.J., Pitz, C.K. Westbrook, D.W., Layton, P.F. Flynn, R.P. Durrett, A.O. zur Loye, O.C. Akinyemi, and F.L. Dryer, Society of Automotive Engineer, No. 2001-01-0653 (2001).

Curran, H.J., Pitz, W.J., Westbrook, C.K., Dagaut, P., Boettner, J-C and Cathonnet, M., "A Wide Range Modeling Study of Dimethyl Ether Oxidation," International Journal of Chemical Kinetics, Vol.30, pp.229-241, 1998.

Dasch, C., "One-dimensional Tomography: a Comparison of Abel, Onion-peeling, and Filtered Backprojection Methods," Applied Optics, Vol. 31, No. 8, pp. 1146–1152 (1992).

Frenklach, M. and Wang, H., "Detailed Modeling of Soot Particle Nucleation and Growth", Twnety-Third Symposium (International) on Combustion, The Combustion Institute, pp.1559-1566, 1990.

Hastie, J. W., and Bonnell, D. W., Molecular Chemistry of Inhibited Combustion Systems, NBSIR 80-2169,1980.

Inal, F. ., S. Senkan, Combustion Science and Technology, 174 (2002) 1-19.

Kohse-Höinghaus, K., and J. Jeffries (Eds.) Applied Combustion Diagnostics. Taylor & Francis, New York, 2002 p. 359-383.

Marinov, N. M, "A Detailed Chemical Kinetic Model for High Temperature Ethanol Oxidation," International Journal of Chemical Kinetics., Vol.31, pp.183-220, 1998.

McBride, B., and S. Gordon, S., Computer Program for Calculation of Complex Chemical Equilibrium Compositions and Applications. NASA Reference Publication 1311, 1996.

McEnally, C.S., Koylu, U.O., Pfefferle, L.D. and Rosener, D.E., "Soot Fraction and Temperature Measurements in Laminar Nonpremixed Flames Using Thermocouple," Combustion and Flame, Vol.109, pp.701-720, 1997.

Mueller, M. , R Yetter, F. Dryer, ChemKinet 31 (1999) 705-724.

Quay, B., The development of laser-induced incandescence for quantitative measurement of soot volume fraction in flames, Ph.D. Thesis, The Pennsylvania State University. (1998)

Santoro, R., Semerjian, H., and Dobbins, R., "Soot Particle Measurements in Diffusion Flames," Combustion and Flame, Vol. 51, pp. 203-218 (1983).

Sgro, L.A., P. Minutolo, G. Basile, A. D'Alessio, Chemosphere 42(5-7) (2001) 671-680.

Song, K., P. Nag, T. Litzinger, D. Haworth, Effects of Oxygenated Additives on aromatic species in fuel-rich, premixed ethane combustion: a modeling study, Combust. Flame 135 (2003) 341-349.

Syred, N., and J.M. Beer, Combustion and Flame, Vol. 23, p. 143-201. (1974)

Xu, F., P. Sunderland, G. Faeth, Soot formation in laminar premixed ethylene/air flames at atmospheric pressure, Combust. Flame 108 (1997) 471-493.